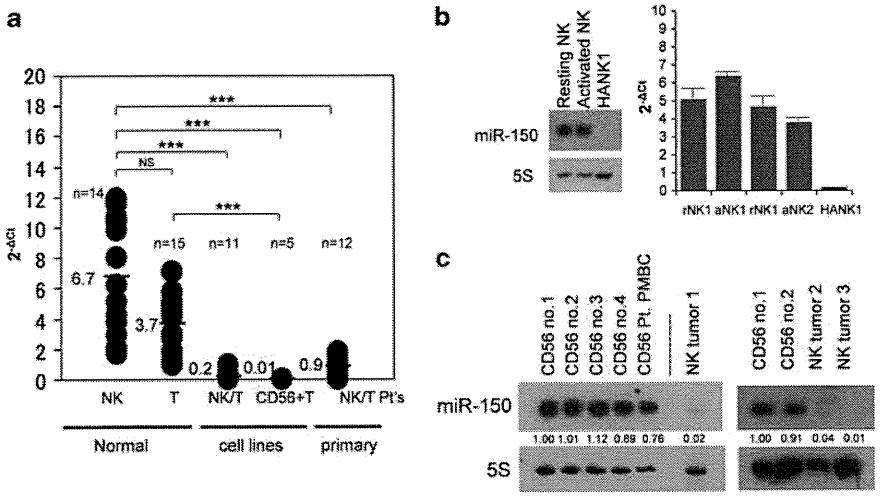

Figure 2 miR-150 expression in primary NK/T-cell lymphoma/leukemia cases. (**a**) Quantitative PCR analysis of miR-150 expression in $sCD3^{-}CD56^{+}$ NK cells (NK, $n=14$), $sCD3^{+}$ T-cells (T, $n=15$), NK-cell lymphoma lines (NK/T, $n=11$), $CD56^{+}$ T-cell lymphoma lines ($CD56^{+}$T, $n=5$) and primary NK/T-cell tumor samples (NK/T patients, $n=12$). The horizontal lines indicate the means. *y* axis, $-\Delta Ct$ values for miRNA expression. Statistical significance: NS, not significant, $^{***}P<0.001$. (**b**) miR-150 expression in resting and activating NK cells. Left panel, Northern blot. Right panel, Taqman PCR. rNK, resting NK. aNK, activated NK. (**c**) Left panel, Northern blot analysis of miR-150 expression in normal resting NK cells (rNK number 1–4, $n=4$), NK cell of a patient and a samples from the patient with NK/T-cell lymphoma, nasal type (described as NK tumor 1). Right panel, Northern blot analysis of miR-150 expression in NK cells ($n=2$) and two patients with NK/T-cell lymphoma, nasal type (NK tumors 2 and 3), whose RNA was also purified from $CD56^{+}$ cells.

2.1%; KAI-3, 3.4%; HANK-1, 5.8%; SNK-6, 6.5%; MOTN-1, 9.7%; Raji, 3.5%; and Daudi, 3.75%. At 14 days later, RNA from the transductants was collected, based on GFP selection (day 0), and subjected to Northern analysis, which showed upregulation of GFP-miR-150 with no changes in the expression of miR-21 or miR-155, as compared with cells transduced with GFP alone (Figure 3a). Quantitative PCR also showed upregulation of miR-150 in all transduced cell lines (Figure 3b). Expressions of miR-150 of all cell lines between normal and GFP^{+} vector-transduced cells showed no differences in the expressions (data not shown).

After initially monitoring % GFP among cells in culture, the conditions for lentiviral infection were adjusted to achieve ~50% GFP-miR-150 positivity among recipient cells (1:1 mixture of ~100% GFP^{+} cells and GFP^{-} cells), after which the mixed cultures were monitored weekly using a flow cytometer. Figure 3c shows the changes in %GFP-miR-150 among HANK-1 cells from day 7 to day 28 after GFP-miR-150 selection. We observed a reduction in %GFP-miR-150 beginning at 14 days after GFP-miR-150 selection, which might have been caused by displacement of GFP^{-} cells. As shown in Figure 3d, a reduction in %GFP-miR-150 was seen in the YT, MOTN-1, HANK-1 and SNK-6 lines, but not in KAI-3 cells or in the two B-cell lymphoma lines, whereas the cell lines transduced with GFP vector did not show the reduction in any cell lines examined. Transduced SNK-6 cells showed a slight upregulation of miR-150 when compared with other transduced cell lines. This effect might be linked to a lower 'decreasing rate (75–80%)' than was seen with the other transduced cells such as MOTN-1 and HANK-1.

miR-150 increases susceptibility to apoptosis and reduces cell proliferation in NK/T-cell lymphoma cell lines

To detect the function of miR-150 during tumorigenesis, we assessed the incidence of apoptosis among transduced cells following exposure to etoposide (100 μM for 4 h) on day 14 after selection. We found that the incidence of apoptosis in the presence of etoposide was increased in MOTN-1 cells (Figure 4a). When we then carried out 5′-bromo-2′-deoxyuridine assays with MOTN-1 cells, we found that the 5′-bromo-2′-deoxyuridine index was significantly reduced in cells transduced with miR-150 (Figure 4b). The same results were obtained in HANK-1 cells (Figures 4c and d). Although SNK-6 cells did not show increased apoptosis when transduced with miR-150 alone, greater numbers of apoptotic cells were detected when the miR-150 was transduced into miR-155 knockdown cells (Figure 5). Similarly, miR-150-positive MOTN-1 and HANK-1 cells expressing ASO-155 did not show a significant increase in the incidence of apoptosis (Supplementary Figure 3). In addition, apoptosis assays with YT cells revealed a cooperative effect between miR-21 and miR-150. YT cells transduced with miR-150 showed significantly larger numbers of apoptotic cells if they were treated with ASO-21 (Figure 5). Moreover, combining miR-150 transduction with miR-21 knockdown induced significant increases in the incidence of apoptosis. In addition, when we carried out 5′-bromo-2′-deoxyuridine assays with SNK-6 and YT cells, we found that the 5′-bromo-2′-deoxyuridine index was significantly reduced in these cells transduced with miR-150 without additive effects (data not shown).

miR-150, thus, appears to function as a tumor suppressor by increasing cell susceptibility to apoptosis and decreasing cell cycle progression, although the effect does not induce a marked reduction in % GFP.

miR-150 induces senescence in NK/T-cell lymphoma lines

We speculated that the reduction in %GFP among miR-150 transductants during culture might reflect cellular senescence. To test this idea, we transduced miR-150 into cells from the YT, MOTN-1, SNK-6 and HANK-1 lines, which had previously showed reductions in %GFP during culture (Figure 3). The miR-150 transduction efficiency was about 5–10%, which was

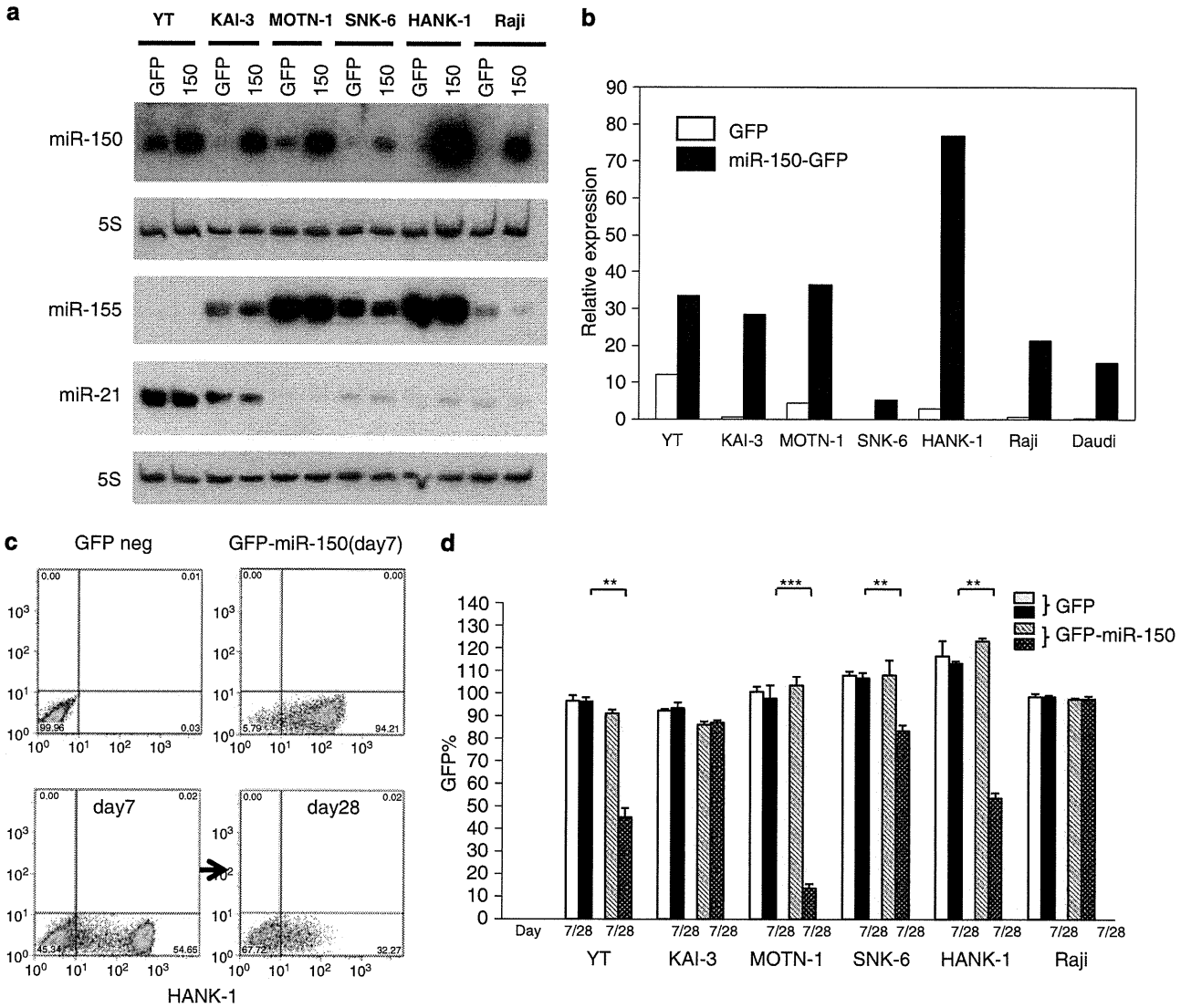

Figure 3 Transduction of miR-150 in lymphoma lines and GFP% monitoring. (**a**) Northern blot analysis of the indicated miRNAs in cells transduced with miR-150 or empty vector (GFP$^+$). The transductant cell type is indicated at the top. Controls (5S tRNA) are shown in the bottom panel. (**b**) Quantitative PCR analysis of miR-150 expression in the indicated cell types transduced with empty vector or miR-150. *y* axis: black and white bars depict $-\Delta Ct$ values for miR-150 expression. *x* axis: cell lines transduced with empty vector (GFP) or miR-150. (**c**) Flow cytometric analysis of the GFP$^+$ fraction (%GFP) among transduced HANK-1 cells. Upper panels: left, GFP$^-$ cells; right, cells transduced with miR-150-GFP (%GFP = approximately 100). Lower panels: left, GFP-miR-150 on day 7 (%GFP = approximately 50); right panel, GFP-miR-150 on day 28. Days: days after GFP-miR-150 selection; alternatively day 0 is at 48 h after GFP-miR-150 transduction. (**d**) %GFP among NK/T-cell lymphoma (YT, KAI-3, MOTN-1, SNK-6 and HANK-1) and Burkitt lymphoma (Raji) lines transduced with GFP-miR-150 or empty vector (GFP). White bars indicate %GFP for GFP transductants on day 7 after GFP selection; black bars, the %GFP for GFP transductants on day 28. Gray bars show the %GFP for GFP-miR-150 transductants on day 7; dark gray bars, the %GFP for GFP-miR-150 transductants on day 28 (YT, MOTN-1, SNK-6 and HANK-1) or day 42 (KAI-3 and Raji). Statistical significance: $^{**}P<0.01$ and $^{***}P<0.001$.

the same as in earlier experiments. After the transduction, GFP$^+$ cells were selected in a cell sorter. We found that the rate of growth of MOTN-1, SNK-6 and HANK-1 cells transduced with miR-150 was lower among cells transduced with empty vector (data of MOTN-1 and HANK-1 are shown in Figure 6a). In addition, these cells stained positively for Ki-67 and senescence-associated beta-gal on day 21 after GFP selection and miR-150 transductants had a 'fried egg'-like appearance, which is caused by senescence and is not seen in normal NK/T-cell lymphoma cells (data of HANK-1 are shown in Figure 6b).

We also used telomeric repeat amplification protocol assays to assess telomerase activity in MOTN-1, SNK-6 and HANK-1 cells, with and without miR-150 transduction, and in normal NK cells. We found that resting and activated NK cells showed no telomerase activity (Figure 6c), whereas NK/T-cell lymphoma cell lines did so, indicating a reverse correlation between expression of miR-150 and telomerase activity (Figure 6c). As shown in Figure 6d, telomerase activity in miR-150 transductants (on day 21 after GFP selection) was markedly lower than in cells transduced with empty vector. Because it is known that lymphocytes without telomerase activity show telomeric DNA shortening during cell culture,[22] we used Southern blot analysis to assess the telomere length in HANK-1, MOTN-1 and SNK-6 cells. Genomic DNA was digested by *Hin*fI, which does not cleave within the repeating (TTAGGG)n sequence that constitutes the telemetric DNA. The lengths of the resultant telemetric

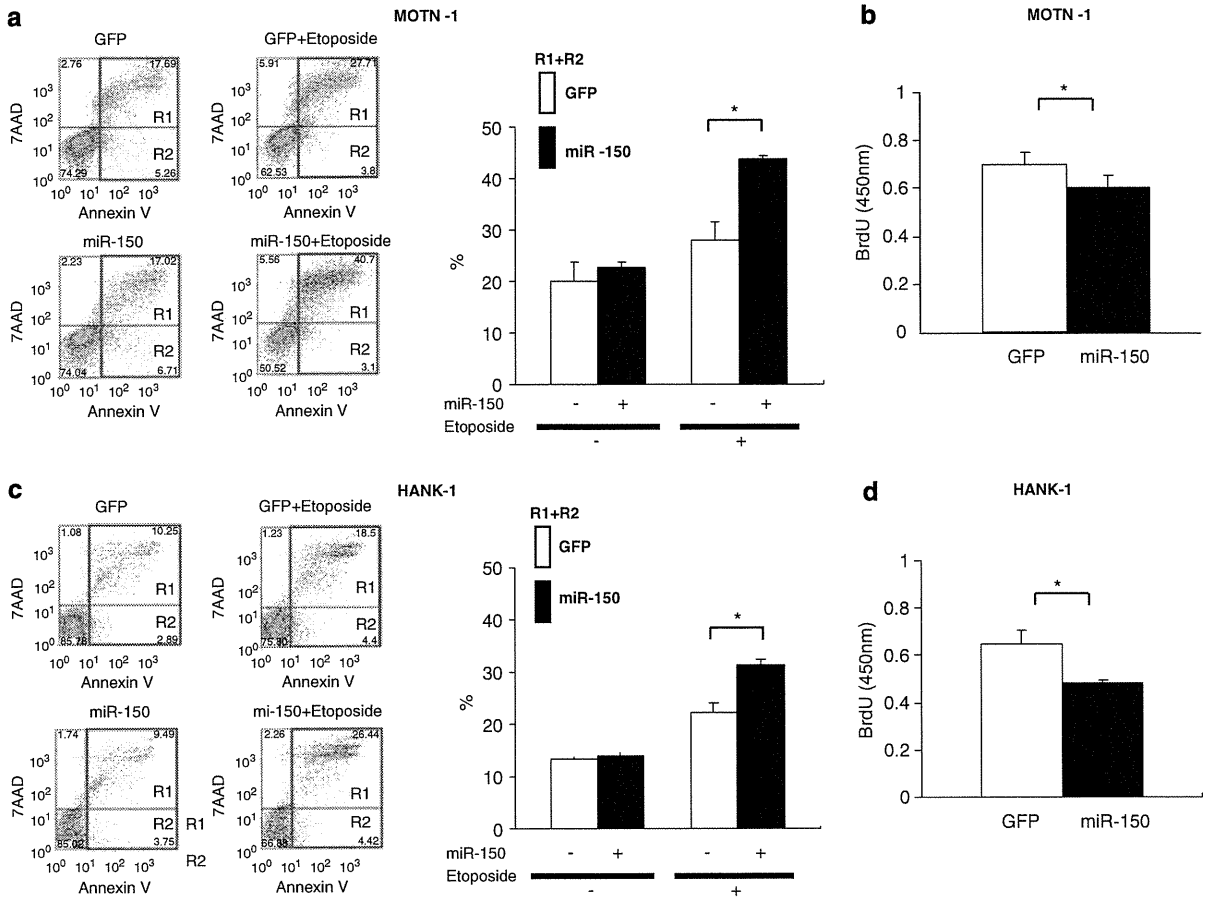

Figure 4 Assays of apoptosis and cell proliferation in miR-150-transduced NK/T-cell lymphoma lines. (**a**) Apoptosis among MOTN-1 cells transduced with miR-150 or empty vector (GFP$^+$). miR-150 transductants were exposed to 100 μM etoposide for 4 h. Left panels: flow cytometric analysis of miR-150 transductants: *y* axis, cells stained by 7-AAD; *x* axis, cells stained by Annexin V-PE. Right panel: Percentages of apoptotic cells (R1 + R2). White and black bars depict percent apoptosis (R1 + R2) among MOTN-1 cell transduced with miR-150. (**b**) Cell proliferation assays (5′-bromo-2′-deoxyuridine assay) in MOTN-1 cells. The white bar shows the 5′-bromo-2′-deoxyuridine index (450 nm) for GFP transductants; the black bar, the 5′-bromo-2′-deoxyuridine index for GFP-miR-150 transductants. (**c**) Apoptosis assays in HANK-1 cells transduced with miR-150 or empty vector (GFP$^+$). (**d**) Cell proliferation assays (5′-bromo-2′-deoxyuridine assay) in HANK-1 cells. The white bar shows the 5′-bromo-2′-deoxyuridine index for GFP transductants; the black bar, the 5′-bromo-2′-deoxyuridine index for GFP-miR-150 transductants. Statistical significance: $*P<0.05$.

restriction fragments were then determined by gel electrophoresis followed by Southern analysis using a probe that recognizes this sequence. As shown in Figure 6e, we observed a shortening of telomeric DNA in the cells expressing miR-150 during continuous culture. Indeed, the telemetric restriction fragments of miR-150 transductants grew shorter with every successive passage (Figure 6f). Thus, miR-150 appears to control aging and senescence in mature lymphocytes.

Identification of direct targets of miR-150 and the downstream targets in NK/T-cell lymphoma

We used Target Scan (http://www.targetscan.org) and Pigtar (http://pictar.mdc-berlin.de) to predict miR-150 targets.[23,24] We then used western analysis to assess expression in various candidate targets, including c-Myb,[25] FOXP1,[26] BCAP (*PIK3AP1*), p85 (*PIK3R1*), AKT2, AKT3, PRL1, Pim1, RECK, Rictor, c-Raf, MSK1, MIB1, ELK1, E2F3 and MLL in MOTN-1, SNK-6 and HANK-1 cells transduced with miR-150 or empty vector. These proteins include upstream mediators of signal transduction, such as AKT, STAT3 and Ras, and might be associated with tumorigenesis when downregulated by forced expression of miR-150. We also analyzed expression of the telomerase-related proteins Dyskerin (gene name dyskeratosis congenita 1, *DKC1*), SirT1, PAI-1, Mre1 and ERCC1, which also possess seed sequences (but not conserved) of miR-150. Of these, loss of Dyskerin function is known to induce senescence.[27] We found that levels of both AKT2 and Dyskerin were reduced in all miR-150 transductants (Figure 7a), whereas BCAP expression was slightly reduced in SNK-6 and HANK-1 cells (data not shown). To determine whether these proteins are direct targets of miR-150, we carried out luciferase reporter assays in Rat-1 fibroblasts stably expressing miR-150. Upon insertion of the wild-type 3′-UTR of *DKC1, PIK3AP1, AKT3* or *AKT2* into the reporter, we observed significant reductions in luciferase activity with *DKC1, PIK3AP1* and *AKT2*, but not in *AKT3* (data not shown), as compared with cells transduced with empty vector (control vector), suggesting that *DKC1, PIK3AP1* (data not shown) and *AKT2* have potential to function as direct targets of miR-150 (Figure 7b).

Overexpression of AKT2 with upregulation of pAKT^{ser474}, which enhances telomerase activity through phosphorylation of human telomerase reverse transcript (hTERT), has been observed in various cancers.[28,29] We therefore carried out a western analysis of pAKT$^{ser473/4}$ expression and found it to be markedly reduced in the cells tested. We also detected upregulation of

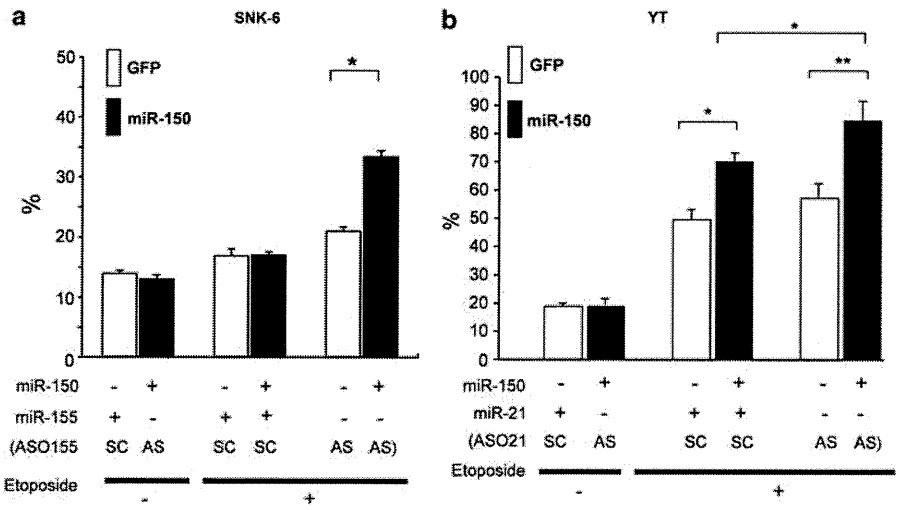

Figure 5 Cooperative effects of miRNAs enhance apoptosis. (**a**) Apoptosis assays in SNK-6 cells transduced with miR-150 or empty vector (GFP^+). Left panel: apoptosis assay. (+) and (−) indicate the presence (+) or absence (−) of miR-155 or miR-150 expressions. ASO-155: cells treated with antisense mR-155 oligo. SC: scramble. AS: antisense. Symbols and bars indicate means and s.d.'s of triplicate samples. Statistical significance: NS, not significant, $*P<0.05$. (**b**) Percentages of apoptotic cells. White and black bars depict percent apoptosis among YT cells transduced with miR-150. (+) and (−) indicate the presence (+) or absence (−) of miR-21 or miR-150 expressions. YT cells show overexpression of miR-21 without expression of miR-155 or miR-150. ASO-21: cells treated with antisense mR-21 oligo. SC: scramble. AS: antisense. Statistical significance: NS, not significant, $*P<0.05$ and $**P<0.01$.

Bim (in MOTN-1, HANK-1 and SNK-6) and p53 (in SNK-6 and HANK-1) (Figure 7c). Bim is a BH3 proapoptotic protein and its upregulation can lead to apoptosis.[30] Upregulation of these tumor suppressors might be linked to pAKT downregulation, although further study will be needed to determine whether or not these changes in expression are pAKT-dependent.

Discussion

Recent studies have shown deregulations of coding genes in NK/T-cell lymphoma.[14,31,32] However, there are no reports of miRNA deregulations in these subtypes. In this study, we assessed miR-150 expression in NK cell and $CD56^+$ T-cell lymphomas, and found it to be significantly reduced. Although aberrantly low expression of miR-150 has been identified in Sezary syndrome,[33] which is classified as a T-cell lymphoma, there have been no reports on its expression and function during NK/T-cell lymphomagenesis. Almost none of the tested cell lines and primary samples of NK/T-cell lymphoma showed expression of miR-150, though mature T and NK cells normally expressed high levels of miR-150,[34] suggesting downregulation miR-150 in lymphomas might be important for lymphomagenesis and contribute to immortalization of the cancer cells. It is also known that normal lymphocytes show senescence with increasing population doublings.[22] Our results suggest that the continuous expression of miR-150 in normal mature lymphocytes may be required to prevent immortalization, which may be a first step toward developing cancer.

Our findings also suggest that downregulation of miR-150 can lead to activation of telomerase via upregulation of AKT2, a prosurvival protein serine/threonine kinase activated via the PI3K pathway, which is a key prosurvival pathway in cancer.[28,29,35–39] Several studies have shown that *AKT2* gene is overexpressed in various tumor cell lines and human malignancies, including B-cell lymphoma, liver, ovarian, pancreatic and breast cancers; and that overexpression of AKT2 protein is associated with increased invasion and metastasis.[35–39] Thus, AKT2 appears to have a crucial role in tumorigenesis.

Activation of the PI3K–AKT pathway through phosphorylation of Serine 474 in AKT2 is strongly associated with tumorigenesis. For example, $pAKT^{ser473/4}$ can upregulate telomerase via phosphorylation of hTERT, resulting in immortalization of cancer cells. Kang *et al*[40] reported that the hTERT subunit has two AKT kinase phosphorylation sites (Ser473 and Thr308 in AKT1/AKT3, Ser474 and Thr309 in AKT2) and that pAKT contributes to telomerase activity through phosphorylation of hTERT. Conversely, inhibition of PI3K–AKT signaling reduces telomerase activity. For example, Plunkett *et al*.[41] reported that, in T cells, the loss of telomerase activity is associated with reduced levels of $pAKT^{ser473/4}$. It is also known that inhibition of AKT signaling by p27 induces a senescence-like arrest, independent of p53.[42] Consistent with those reports, our results strongly suggest that activation (phosphorylation) of AKT due to the loss of miR-150 expression may have a key role in enhancing human telomerase activity in the cancer cells.

Interestingly, forced expression of miR-150 can also lead to downregulation of *DKC1*/Dyekerin in NK/T-cell lymphoma cells, suggesting that loss of miR-150 may activate Dyskerin. It is encoded by *DKC1* and is a predominantly nucleolar protein essential for the formation of pseudouridine in RNA and the telomerase RNA subunit hTR.[43,44] Dyskeratosis congenita patients have a nonsense mutation within *DKC1*, leading to diminished expression of Dyskerin accompanied by downregulation of telomerase activity.[45] Overexpression of *DKC1* has been seen in solid tumors, and the silencing of *DKC1* can reduce telomerase activity and rRNA pseudouridylation.[46,47] These findings suggest that the level of Dyskerin expression parallels the activation and inactivation of telomerase. Together, activation of hTERT via pAKT and the continuous expression of Dyskerin could contribute to the enhancement of telomerase activity; however, it is still unclear whether the reduced expression of Dyskerin leads directly to inactivation of telomerase or whether telomerase is regulated via miR-150 itself.

In the present study, we do not address the mechanism underlying the loss of miR-150 expression in NK/T-cell

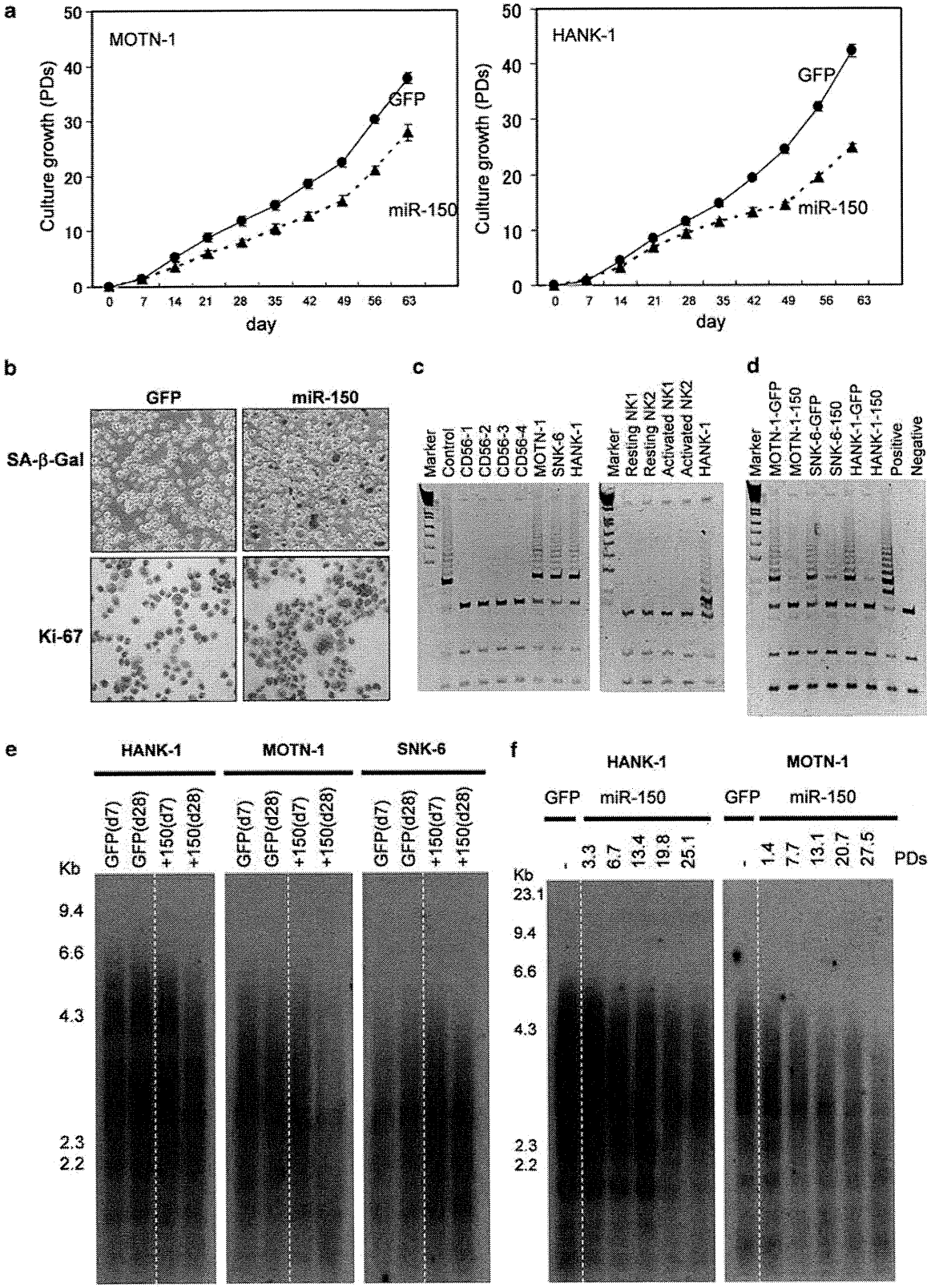

Figure 6 miR-150 induces senescence in NK/T-cell lymphoma lines. (**a**) Cell growth assay in MOTN-1 and MOTN-1 cells. PDs, population doublings. Days, days after GFP-miR-150 selection; alternatively day 0 is at 48 h after GFP-miR-150 transduction. (**b**) Senescence assay in HANK-1 cells. Upper panels: senescence-associated beta-gal assay. Lower panels: Ki-67 staining of HANK-1 cells transduced with empty vector (GFP) or miR-150. (**c**) Telomerase activity in NK cells and NK-cell lymphoma lines. Left panel: telomeric repeat amplification protocol assay with normal NK-cells (four samples) and NK-cell lymphoma lines (MOTN-1, SNK-6 and HANK-1). Right panel: telomeric repeat amplification protocol assay with resting (rNK) and activated NK cells (aNK) and HANK-1 cells. (**d**) Telomerase activity (TRAP assay) in NK cells transduced with empty vector (GFP) or miR-150. (**e**) Southern blot analysis of HANK-1, MOTN-1 and SNK-6 cell lines, with (day 7) and without (day 28) miR-150 expression. (**f**) Changes in telomere length in HANK-1 and MOTN-1 cells with PDs. GFP, cells transduced with empty vector. miR-150, NK-cell lymphoma cells transduced with miR-150.

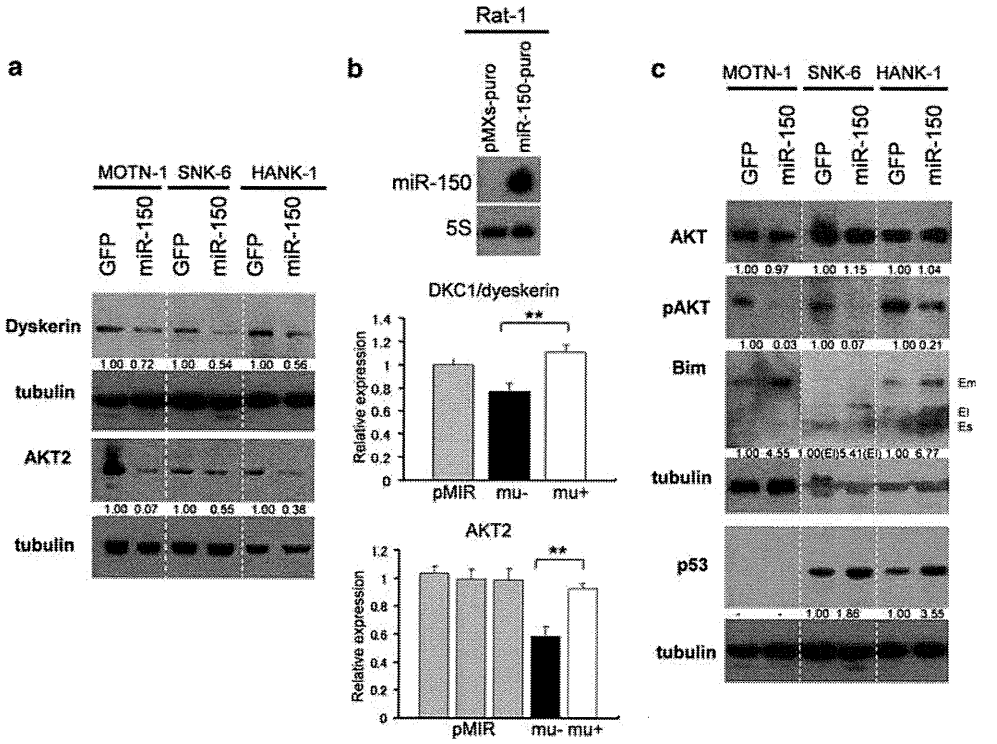

Figure 7 Luciferase assay of miR-150 targets and the expression of downstream AKT. (**a**) Western blot analysis of Dyskerin (*DKC1*) and AKT2 expression in MOTN-1, SNK-6 and HANK-1 cells in the presence or absence of miR-150 expression. (**b**) Luciferase reporter assays of *AKT2* and *DKC1* expression in Rat-1 cells transfected with miR-150 or empty vector (pMIR). Blots showing miR-150 expression are beside the bars. Statistical significance: NS, not significant, $^{**}P<0.01$. (**c**) Western analysis of $pAKT^{ser473/4}$ expression and expression of its downstream targets. MOTN-1, SNK-6 and HANK-1 cells transduced without (GFP) and with miR-150 are lined. Examined downstream proteins are Bim and p53. Fold changes in protein levels are shown below the gels and are normalized to the level in the respective miR-150-transduced cell lines, which were assigned a value of 1.00.

lymphomas. We can say, however, that it is likely not the result of genomic alteration and/or an epigenetic mechanism, such as deletion or methylation/deacetylation. Fluorescence *in situ* hybridization analysis of 19q31.33 in all eleven NK/T-cell lymphoma cell lines revealed no genomic deletion, and 5-Aza-2′-deoxycydine (a DNA methyltransferase inhibitor) and/or trichostatin A (a histone deacetylase inhibitor) did not restore miR-150 activity in these lymphoma cells (data not shown). Previously, Chang *et al.*[48] showed that miR-150 is downregulated by c-Myc and that miR-150 may function as a tumor suppressor, asw injection of mouse lymphoma cell lines into mice expressing miR-150 produced fewer tumor cells *in vivo*. We used Northern and western blot analyses to examine c-Myc expression in NK (YT, KAI-3, MOTN-1, SNK-6 and HANK-1) and B-cell (Raji and Daudi) lymphoma lines (these cell lines showed no expression of miR-150). Although the B-cell lymphoma lines strongly expressed c-Myc, two (KAI-3, and YT) of the five NK-cell lymphoma lines did not express c-Myc (Supplementary Figure 4). Given that these two cell lines also did not express miR-150, it is not likely that the downregulation of miR-150 was due to c-Myc, at least not in these cells. This suggests there is another regulator of miR-150.

We previously demonstrated that miR-21 and/or miR-155 are overexpressed in NK-cell lymphomas.[13] These miRNAs, respectively, downregulate the phosphatases PTEN and SHIP1, leading to activation of the PI3K–AKT pathway. In earlier studies[13] and the present one, we found that miR-21 could function as an oncomiR by enhancing anti-apoptotic activity in NK-cell tumors, and that the effect was strengthened when miR-21 functioned cooperatively with miR-150. Our findings also indicate that transduction of miR-155 alone did not increase oncogenic activity, despite a slight upregulation of pAKT. However, our observation that knockdown of miR-155 alone increased the incidence of apoptosis cells when it was expressed with miR-150 suggests that miR-155 may serve as an oncomiR, though its activity is weaker than that of miR-21 or miR-150. This suggests miR-155 may function as an enhancer of oncomiRs in NK cell tumors. Our earlier findings showed that expression of miR-21 and miR-155 is mutually exclusive in both NK cell lines and primary tumors from patients.[13] In the present study, we found that miR-150 is downregulated in both NK cell lines and primary tumors. These oncomiRs may function cooperatively to enable the continuous activation of PI3K–AKT signaling, ultimately leading to enhancing anti-apoptotic activity, cell cycle progression, cell proliferation and immortalization via targeting of downstream mediators such as hTERT, p53 and Bim.

In summary, we have shown that miR-150 functions as a tumor suppressor in NK/T-cell lymphomas. Our results also suggest that miR-150 likely serves as an upstream regulator of the PI3K–AKT pathway. These findings could provide a basis for new therapies targeting AKT in the treatment of NK/T-cell lymphoma.

Conflict of interest

The authors declare no conflict of interest.

Acknowledgements

This work is supported in by a Grant-in-Aid from the Japan Society for the Promotion of Science (HT). We wish to express our appreciation to Ms E Kobayashi, Y Abe, Y Chiba and H Kataho for their outstanding technical assistance, Dr T Nanjo (Akita University, Akita, Japan) and Dr R Ichinohasama (Tohoku University,
Sendai, Japan) for their histological and/or clinical diagnosis of lymphoma. Antibody against BCAP was kindly provided from Professor T Kurosaki (RIKEN). pMX vector was kindly provided by Dr T Kitamura (Tokyo University, Tokyo, Japan).

Author contributions

AW performed all experiments, analyzed data, designed experiments and constructed figures and tables. HT designed and performed experiments, analyzed data, wrote the paper and organized the study. JY, KT, MN, KI, MK, YK, NT, TN, SN and KS performed experiments and analyzed data.

References

1 Jaffe ES, Harris NL, Stein H, Campo E, Pileri SA, Swerdlow SH. Introduction and over review of the classification of the lymphoid neoplasms. In: Swerdloe, A.H., Campo E, Harris NL, Jaffe ES, Stein H, Thiele J, Vardiman JW (eds). *World Health Organization Classification of Tumors of Haematopoietic and Lymphoid Tissues.* IARC press: Lyon, Washington, 2008, pp 158–178.
2 Siu LL, Wong KF, Chan TK, Kwong YL. Comparative genomic hybridization analysis of natural killer cell lymphoma. *Am J Pathol* 1999; **155**: 1419–1425.
3 Siu LLP, Chan V, Chan JKC, Wong KF, Liang R, Kwong YL. Consistent patterns of allelic loss in natural killer cell lymphoma. *Am J Pathol* 2000; **157**: 1803–1809.
4 Wong KF, Zhang YM, Chan JK. Cytogenetic abnormalities in natural killer cell lymphoma/leukemia: is there a consistent pattern? *Leuk Lymphoma* 1999; **34**: 241–250.
5 Yoon J, Ko YH. Deletion mapping of the long arm of chromosome 6 in peripheral T and NK cell lymphomas. *Leuk Lymphoma* 2003; **44**: 2077–2082.
6 Ko YH, Choi KE, Han JH, Kim JM, Ree HJ. Comparative genomic hybridization study of nasal-type NK/T-cell lymphoma. *Cytometry* 2001; **46**: 85–91.
7 Nakashima Y, Tagawa H, Suzuki R, Karnan S, Karube K, Ohshima K *et al.* Genome-wide array-based comparative genomic hybridization of natural killer cell lymphoma/leukemia: different genomic alteration patterns of aggressive NK-cell leukemia and extranodal NK/T cell lymphoma, nasal type. *Genes Chromosomes Cancer* 2005; **44**: 247–255.
8 Iqbal J, Kucuk C, Deleeuw RJ, Srivastava G, Tam W, Geng H *et al.* Genomic analyses reveal global functional alterations that promote tumor growth and novel tumor suppressor genes in natural killer-cell malignancies. *Leukemia* 2009; **23**: 1139–1151.
9 Bartel DP. MicroRNAs: genomics, biogenesis, mechanism, and function. *Cell* 2004; **116**: 281–297.
10 Iorio MV, Croce CM. MicroRNAs in cancer: small molecules with a huge impact. *J Clin Oncol* 2009; **27**: 5848–5856.
11 Croce CM. Causes and consequences of microRNA dysregulation in cancer. *Nat Rev Genet* 2009; **10**: 704–714.
12 Esquela-Kerscher A, Slack FJ. Oncomirs-microRNAs with a role in cancer. *Nat Rev Cancer* 2006; **6**: 259–269.
13 Yamanaka Y, Tagawa H, Takahashi N, Watanabe A, Guo Y-M, Iwamoto K *et al.* Aberrant overexpression of microRNAs activate AKT signaling via down-regulation of tumor suppressors in natural killer-cell lymphoma/leukemia. *Blood* 2009; **114**: 3265–3275.
14 Huang Y, de Reynies A, de Leval L, Ghazi B, Martin-Garcia N, Travert M *et al.* Gene expression profiling identifies emerging oncogenic pathways operating in extranodal NK/T-cell lymphoma, nasal type. *Blood* 2010; **115**: 1226–1237.
15 Kagami Y, Nakamura S, Suzuki R, Iida S, Yatabe Y, Okada Y *et al.* Establishment of an IL-2-dependent cell line derived from 'nasal-type' NK/T-cell lymphoma of CD2+, sCD3-, CD3e+, CD56+ phenotype and associated with the Epstein-Barr virus. *Br J Haematol* 1998; **103**: 669–677.
16 Nagata H, Konno A, Kimura N, Zhang Y, Kimura M, Demachi A *et al.* Characterization of novel natural killer (NK)-cell and gamma delta T cell lines established from primary lesions of nasal T/NK cell lymphomas associated with the Epstein-Barr virus. *Blood* 2001; **97**: 708–713.
17 Matsuo Y, Drexler HG, Takeuchi M, Tanaka M, Orita K. Establishment of the T-cell large granular lymphocyte leukemia cell line MOTN-1 carrying natural killer-cell antigens. *Leukemia Res* 2002; **26**: 873–879.
18 Zhang Y, Nagata H, Ikeuchi T, Mukai H, Oyoshi MK, Demachi A *et al.* Common cytological and cytogenetic features of Epstein-Barr virus (EBV)-positive natural killer (NK) cells and cell lines derived from patients with nasal T/NK-cell lymphomas, chronic active EBV infection and hydroa vacciniforme-like eruptions. *Br J Haematol* 2003; **121**: 805–814.
19 Inomata M, Tagawa H, Guo YM, Kameoka Y, Takahashi N, Sawada K. MicroRNA-17–92 down regulates expression of distinct targets in different B-cell lymphoma subtypes. *Blood* 2009; **113**: 396–402.
20 Chen C-Z, Li L, Lodish HF, Bartel DP. MicroRNA modulate hematopoietic linage differentiation. *Science* 2004; **303**: 83–86.
21 Merkerova M, Belickova M, Brucova H. Differential expression of microRNAs in hematopoietic cell linages. *Eur J Haematol* 2008; **81**: 304–310.
22 Counter CM, Botelho FM, Wang P, Harley CB, Bacchetti S. Stabilization of short telomeres and telomerase activity accompany immortalization of Epstein-Barr virus-transformed human B lymphocytes. *J Virol* 1994; **68**: 3410–3414.
23 Lewis BP, Shih IH, Rhoades MW, Bartel DP, Burge CB. Prediction of mammalian microRNA targets. *Cell* 2003; **115**: 787–798.
24 Krek A, Grün D, Poy MN, Wolf R, Rosenberg L, Epstein EJ *et al.* Combinational microRNA target predictions. *Nat Genet* 2005; **37**: 495–500.
25 Xiao C, Calado DP, Galler G, Thai TH, Patterson HC, Wang J *et al.* MiR-150 controls B cell differentiation by targeting the transcription factor c-Myb. *Cell* 2007; **131**: 146–159.
26 Tan LP, Wang M, Robertus JL, Schakel RN, Gibcus JH, Diepstra A *et al.* miRNA profiling of B-cell subsets: specific miRNA profile for germinal center B cells with variation between centroblasts and centrocytes. *Lab Invest* 2009; **89**: 708–716.
27 Mitchell JR, Wood E, Collins K. A telomerase component is defective in the human disease dyskeratosis congenita. *Nature* 1999; **402**: 551–555.
28 Testa JR, Bellacosa A. AKT plays a central role in tumorigenesis. *Proc Natl Acad Sci USA* 2001; **98**: 10983–10985.
29 Vivanco I, Sawyers CL. The phosphatidylinositol 3-kinase AKT pathway in human cancer. *Nat Rev Cancer* 2002; **2**: 489–501.
30 O'Connor L, Strasser A, O'Reilly LA, Hausmann G, Adams JM, Cory S *et al.* Bim: a novel member of the Bcl-2 family that promotes apoptosis. *EMBO J* 1998; **17**: 384–395.
31 Iqbal J, Weisenburger DD, Chowdhury A, Tsai MY, Srivastava G, Greiner TC *et al.* Natural killer cell lymphoma shares strikingly similar molecular features with a group of non-hepatosplenic γδ T-cell lymphoma and is highly sensitive to a novel aurora kinase A inhibitor *in vitro*. *Leukemia* 2011; **25**: 348–358.
32 Ng SB, Selvarajan V, Huang G, Zhou J, Feldman AL, Law M *et al.* Activated oncogenic pathways and therapeutic targets in extranodal nasal-type NK/T cell lymphoma revealed by gene expression profiling. *J Pathol* 2011; **223**: 496–510.
33 Ballabio E, Mitchell T, van Kester MS, Taylor S, Dunlop HM, Chi J *et al.* MicroRNA expression in Sezary syndrome: identification, function, and diagnostic potential. *Blood* 2010; **116**: 1105–1113.
34 Zhou B, Wang S, Mayr C, Bartel DP, Lodish HF. miR-150, a microRNA expressed in mature B and T cells, blocks early B cell development when expressed prematurely. *Proc Natl Acad Sci USA* 2007; **104**: 7080–7085.
35 Arranz E, Robledo M, Martinez B, Gallego J, Roman A, Rivas C *et al.* Incidence of homogeneously staining regions in non-Hodgkin lymphomas. *Cancer Genet Cytogenet* 1996; **87**: 1–3.

36 Xu X, Sakon M, Nagano H, Hiraoka N, Yamamoto H, Hayashi N *et al.* Akt2 expression correlates with prognosis of human hepatocellular carcinoma. *Oncol Rep* 2004; **11**: 25–32.
37 Thompson FH, Nelson MA, Trent JM, Guan XY, Liu Y, Yang JM *et al.* Amplification of 19q13.1-q13.2 sequences in ovarian cancer. G-band, FISH, and molecular studies. *Cancer Genet Cytogenet* 1996; **87**: 55–62.
38 Cheng JQ, Ruggeri B, Klein WM, Sonoda G, Altomare DA, Watson DK *et al.* Amplification of AKT2 in human pancreatic cells and inhibition of AKT2 expression and tumorigenicity by antisense RNA. *Proc Natl Acad Sci USA* 1996; **93**: 3636–3641.
39 Arboleda MJ, Lyons JF, Kabbinavar FF, Bray MR, Snow BE, Ayala R *et al.* Overexpression of AKT2/protein kinase B beta leads to up-regulation of beta1 integrins, increased invasion, and metastasis of human breast and ovarian cancer cells. *Cancer Res* 2003; **63**: 196–206.
40 Kang SS, Kwon T, Kwon DY, Do SI. Akt protein kinase enhances human telomerase activity through phosphorylation of telomerase reverse transcriptase subunit. *J Biol Chem* 1999; **274**: 13085–13090.
41 Plunkett FJ, Franzese O, Finney HM, Fletcher JM, Belaramani LL, Salmon M *et al.* The loss of telomerase activity in highly differentiated CD8+CD28-CD27-T cells is associated with decreased Akt (Ser473) phosphorylation. *J Immunol* 2007; **178**: 7710–7719.
42 Collado M, Medema RH, Garcia-Cao I, Dubuisson HLN, Barradas M, Glassford J *et al.* Inhibition of the phosphoinositide 3-kinase pathway induces a senescence-like arrest mediated by p27Kip1. *J Biol Chem* 2002; **275**: 21960–21968.
43 Heiss NS, Knight SW, Vulliamy TJ, Klauck SM, Wiemann S, Mason SPJ *et al.* X-linked dyskeratosis congenita is caused by mutations in a highly conserved gene with putative nucleolar functions. *Nat Genet* 1998; **19**: 32–38.
44 Mitchell JR, Wood E, Collins K. A telomerase component is defective in the human disease dyskeratosis congenita. *Nature* 1999; **402**: 551–555.
45 Sieron P, Hader C, Hatina J, Engers R, Wlazlinski A, Muller M *et al.* DKC1 overexpression associated with prostate cancer progression. *Br J Cancer* 2009; **101**: 1410–1416.
46 Montanaro L, Brigotti M, Clohessy J, Barbieri S, Ceccarelli C, Santini D *et al.* Dyskerin expression influences the level of ribosomal RNA pseudo-uridylation and telomerase RNA component in human breast cancer. *J Pathol* 2006; **210**: 10–18.
47 Montanaro L, Calienni M, Ceccarelli C, Santini D, Taffurelli M, Pileri S *et al.* Relationship between dyskerin expression and telomerase activity in human breast cancer. *Cell Oncol* 2008; **30**: 483–490.
48 Chang TC, Yu D, Lee YS, Wentzel EA, Arking DE, West KM *et al.* Widespread microRNA repression by Myc contributes to tumorigenesis. *Nat Genet* 2008; **40**: 43–50.

Supplementary Information accompanies the paper on the Leukemia website (http://www.nature.com/leu)

Jpn J Ophthalmol (2011) 55:495–501
DOI 10.1007/s10384-011-0065-8

CLINICAL INVESTIGATION

Diagnosis of ocular toxoplasmosis by two polymerase chain reaction (PCR) examinations: qualitative multiplex and quantitative real-time

Sunao Sugita · Manabu Ogawa · Shizu Inoue · Norio Shimizu · Manabu Mochizuki

Received: 26 December 2010 / Accepted: 19 April 2011 / Published online: 13 July 2011

Abstract
Aim To establish a two-step polymerase chain reaction (PCR) diagnostic system for ocular toxoplasmosis.
Methods A total of 13 ocular fluid samples (11 aqueous humor and 2 vitreous fluid) were collected from 13 patients with clinically suspected ocular toxoplasmosis. Ten ocular samples from other uveitis patients and 20 samples from subjects without ocular inflammation were used as controls. Two polymerase chain reaction (PCR) methods, i.e., qualitative multiplex PCR and quantitative real-time PCR, were used to measure the toxoplasma genome (*T. gondii* B1 gene).
Results Qualitative multiplex PCR detected *T. gondii* B1 gene in the ocular fluids of 11 out of 13 patients with clinically suspected ocular toxoplasmosis. In real-time PCR, we detected high copy numbers of *T. gondii* DNA (5.1×10^2–2.1×10^6 copies/mL) in a total of 10 patients (10/13, 77%). Only ocular toxoplasmosis scar lesions were observed in the three real-time PCR-negative patients. PCR assay results for the samples from the two control groups were all negative.
Conclusions The two-step PCR examination to detect toxoplasma DNA is a useful tool for diagnosing ocular toxoplasmosis.

S. Sugita (✉) · M. Ogawa · S. Inoue · M. Mochizuki
Department of Ophthalmology and Visual Science, Tokyo Medical and Dental University Graduate School of Medicine, 1-5-45 Yushima, Bunkyo-ku, Tokyo 113-8519, Japan
e-mail: sunaoph@tmd.ac.jp

N. Shimizu
Department of Virology, Medical Research Institute, Tokyo Medical and Dental University Graduate School of Medicine and Dental Sciences, Tokyo, Japan

Keywords Ocular toxoplasmosis · Polymerase chain reaction · Uveitis · Ocular fluids

Introduction

Ocular toxoplasmosis is a sight-threatening intraocular inflammatory disorder prevalent in many parts of the world. In clinical practice, ocular toxoplasmosis diagnosis is made based on *Toxoplasma gondii* (*T. gondii*) serological tests and on the findings of typical ocular manifestations, for example old retinal necrotic lesions with pigmentation and fresh retinal lesions adjacent to chorioretinal atrophic lesions. However, there are many asymptomatic sero-positive individuals in the area in which *T. gondii* is endemic, with atypical lesions of ocular toxoplasmosis that resemble other necrotizing retinitis, for example acute retinal necrosis and cytomegalovirus retinitis. It is, therefore, necessary to perform laboratory tests to confirm toxoplasmosis infections in the eye. Ocular fluids, which include the aqueous humor and vitreous fluid, are ideal samples for this test, because they can be used to examine local specific antibody production (Goldmann–Witmer coefficient; GWC) or *T. gondii* DNA by polymerase chain reaction (PCR). Previous reports reveal that GWC and PCR assays performed on ocular samples can play a prominent role in the diagnosis of *Toxoplasma* infections [1–12]. Because local specific antibody production is often unpredictable in immunocompromised patients, the PCR assay is reported to be a better diagnostic tool [10]. In addition, the PCR assay can also be used to examine ocular samples for the purpose of diagnosing ocular toxoplasmosis in immunocompetent patients [11] and the atypical strain of *T. gondii* [12]. Moreover, previous studies found that PCR is a rapid and sensitive method

for detecting *T. gondii* quantitatively in clinical specimens [13–16]. However, no previous studies have screened other pathogenic agents that could cause necrotizing retinitis in conjunction with *T. gondii*.

In this study, we attempted to measure the *Toxoplasma* genome in ocular samples of patients with clinically suspected ocular *Toxoplasma* by using a two-step PCR system with specific primers and probes for *T. gondii* DNA amplification (*T. gondii* B1 gene). To screen for the human herpes virus and *T. gondii*, the first step used qualitative multiplex PCR to detect the toxoplasma genome in the ocular sample. In the second step, quantitative real-time PCR was used to measure the genomic DNA of *T. gondii*.

Materials and methods

Subjects

This research followed the tenets of the Declaration of Helsinki, with the study protocol approved by the Institutional Ethics Committee of Tokyo Medical and Dental University. Ocular fluid samples were collected only after each patient had provided written informed consent.

Table 1 summarizes the clinical findings observed for patients with ocular toxoplasmosis at their initial presentation. The first patient group was examined between January 2008 and September 2010 at the Tokyo Medical and Dental University Hospital. This group included 13 consecutive patients clinically suspected of having ocular toxoplasmosis based on the serological test for *T. gondii* (serum anti-Toxo IgG: PHA method) and characteristic ocular manifestations. Of these 13 patients, 10 had active intraocular inflammation, that is, there were anterior chamber cells, vitreous opacity, retinal vasculitis, and fresh retinal exudates (focal retinal necrosis). For the other 3 patients, only inactive ocular toxoplasmosis lesions in the form of old pigmented retinal scars were found. For the PCR assay, we collected intraocular fluids from 13 patients (11 aqueous humor and 2 vitreous fluids).

In the second group, we collected 10 samples (8 aqueous humor and 2 vitreous fluid) from 10 patients with other clinical entities of uveitis. The diagnoses for the subjects included idiopathic uveitis ($n = 7$), acute retinal necrosis ($n = 2$), and cytomegalovirus retinitis ($n = 1$). At the time of sampling, all members of this group had active intraocular inflammation.

In the third group, we collected 20 samples (15 aqueous humor and 5 vitreous fluid) from 20 patients with non-inflammatory diseases. The patient diagnoses included age-related cataract ($n = 15$), primary rhegmatogenous retinal detachments ($n = 1$), idiopathic macular hole ($n = 1$), and idiopathic epiretinal membranes ($n = 3$).

The sampling procedures were performed in accordance with the method reported in our previous studies [17–19]. Briefly, we used surgical microscopy to aseptically collect aliquots of approximately 0.1 ml aqueous humor in a syringe with a 30 G needle. Non-diluted vitreous fluid (approximately 0.5 ml) was collected during the pars plana vitrectomy.

Polymerase chain reaction

DNA was extracted from samples by use of a DNA Mini Kit (Qiagen, Valencia, CA, USA) installed on a robotic workstation for automated purification of nucleic acids (BioRobot E21, Qiagen). For the DNA extraction, approximately 0.1 ml aqueous humor and 0.2 ml vitreous fluid were used. DNA was eluted with 60 μl elution buffer, the amount of DNA used for PCR was 5 μl.

For the PCR assay, we used standard toxoplasma DNA strains for the *T. gondii* RH strains. To detect the toxoplasma genome (*T. gondii* B1 gene), we used two PCR assays, the qualitative multiplex PCR and the quantitative real-time PCR. Multiplex PCR was designed to qualitatively detect genomic DNA of human herpes viruses, i.e., herpes simplex virus type 1 (HSV-1) and type 2 (HSV-2), varicella zoster virus (VZV), Epstein–Barr virus (EBV), cytomegalovirus (CMV), and human herpes virus type 6 (HHV6), type 7 (HHV7), and type 8 (HHV8). PCR was performed using a LightCycler (Roche, Basel, Switzerland). Primers and probes of HHV1-8 and the PCR conditions have been described elsewhere [17, 18]. In addition to the herpes virus PCR, we calibrated the primers and the probe for detecting toxoplasma DNA (*T. gondii* B1 gene) as shown in Table 2. Specific primers for the virus were used with AccuPrime Taq (Invitrogen, Carlsbad, CA, USA). Products were subjected to 40 cycles of PCR amplification. Hybridization probes were then mixed with the PCR products. Real-time PCR was only performed for *T. gondii* when the genomic DNA of *T. gondii* was detected by multiplex screening PCR.

The real-time PCR was performed using AmpliTaq Gold and the Real-Time PCR 7300 system (Applied Biosystems, Foster City, CA, USA). The PCR conditions used for the *T. gondii* B1 gene were: 95°C for 0 s and 60°C for 20 s for 50 cycles. The PCR conditions used for the human herpes viruses have been described elsewhere [17, 18]. When more than 10 copies/mL were detected, the sample copy number was regarded as significant.

Results

Figure 1 shows representative PCR data (Case 1, Table 3). The multiplex PCR performed in order to screen all 8

Table 1 Clinical findings at initial presentation for patients with ocular toxoplasmosis

Case	Age	Sex	Eye	Initial findings and inflammation of AC					Duration of the symptoms	Vitreitis	Retinal vasculitis	Retinal exudates	
				VA	IOP (mmHg)	Granulomatous KPs	AC: cell	AC: flare				Old	Fresh
1	58	M	L	0.1	19	+	3+	131	2 months	+	+	+	+
2	70	F	L	0.3	21	+	2+	76	3 weeks	+	−	+	+
3	68	F	R	0.8	14	−	2+	34	2 months	+	+	−	+
4	44	M	R	1.0	12	+	1+	17	1.5 months	+	−	+	+
5	56	M	L	0.7	22	+	2+	43	3 weeks	+	+	+	+
6	65	F	L	1.0	15	+	1+	26	2 weeks	+	−	−	+
7	48	M	R	0.4	14	+	3+	124	3 weeks	+	+	+	+
8	35	M	L	0.6	18	−	1+	14	1 month	+	+	+	+
9	49	M	L	0.9	18	+	2+	29	1 month	+	+	+	+
10	59	F	R	0.5	20	−	1+	23	1.5 months	+	−	+	+
11	47	M	R	1.2	17	−	−	8	None	−	−	+	−
12	53	F	L	1.2	13	−	−	12	None	−	−	+	−
13	71	M	R	0.9	16	−	−	11	None	−	−	+	−

All patients were immunocompetent. "Old retinal exudates" indicates inactive ocular toxoplasmosis lesions in the form of old pigmented retinal scars

VA visual acuity, *IOP* intraocular pressure, *KPs* keratic precipitates, *AC* anterior chamber

Table 2 Design of primers and probe for detecting toxoplasma DNA (*T. gondii* B1 gene)

For multiplex PCR (qualitative PCR)
Primer F—TCCCCTCTGCTGGCGAAAAGT
Primer R—AGCGTTCGTGGTCAACTATCGATTG
LCRed640—GGTGTATTCGCAGATTGGTCGCCTG-P
Probe—CGAAAAGTGAAATTCATGAGTATCTGTG CAACT-6FAM
For Real-time PCR (quantitative PCR)
Primer F—TCCCCTCTGCTGGCGAAAAGT
Primer R—AGCGTTCGTGGTCAACTATCGATTG
Probe—6FAM-TCTGTGCAACTTTGGTGTATTCGCAG-iowaBK

We designed the primers and probes for the multiplex PCR and real-time PCR. The design of the primers is the same for the two PCR methods, although the relative positions of the TaqMan probe in the B1 gene were changed

human herpes virus DNAs and the *T. gondii* DNAs were positive for the *T. gondii* DNA (Fig. 1a). However, this sample was negative for all human herpes virus DNA tests. In addition, quantitative real-time PCR revealed that there were 1.1×10^6 copies/mL of *T. gondii* DNA in this specimen (Fig. 1b). Figure 2 shows the ocular findings for the patient. At the initial presentation, we made a clinical diagnosis of ocular toxoplasmosis based on both the clinical features and the serological tests (serum anti-Toxo IgG: ×640). Based on these findings, we treated the patient with systemic acetylspiramycin and prednisolone for 3 months. The treatment was effective and the active ocular lesions in the left eye completely disappeared. Two months after the treatment, a subsequent PCR indicated that the *T. gondii* DNA in the aqueous humor sample was now undetectable.

Table 3 summarizes the PCR results. Qualitative multiplex PCR for the *T. gondii* B1 gene was positive for 11 out of 13 patients with clinically suspected ocular toxoplasmosis (Table 3). Real-time PCR detected the B1 gene but not the human herpes virus DNA in the 10 patients who were clinically suspected of having ocular toxoplasmosis (10/13, 77%). In addition, high copy numbers of *T. gondii* DNA were detected (5.1×10^2–2.1×10^6 copies/mL) in all of these 10 patients, with active ocular inflammatory lesions that were compatible with ocular toxoplasmosis, i.e., focal retinal necrosis, vitreous opacity, anterior chamber cells, and choroidal edema with possible old scars. The only factors in the three PCR-negative patients that were compatible with an ocular toxoplasmosis diagnosis were the inactive scar lesions, i.e., old pigmented retinal scars. Of note is the finding that in one of these three patients *T. gondii* DNA was detected by the multiplex qualitative PCR in the aqueous humor sample (Case 12 in Table 3), even though the real-time PCR showed negative results (<10 copies/mL). A fundus photograph of a patient with inactive ocular toxoplasmosis is seen in Fig. 3. For this particular patient (Case 11 in Table 3), the PCR results

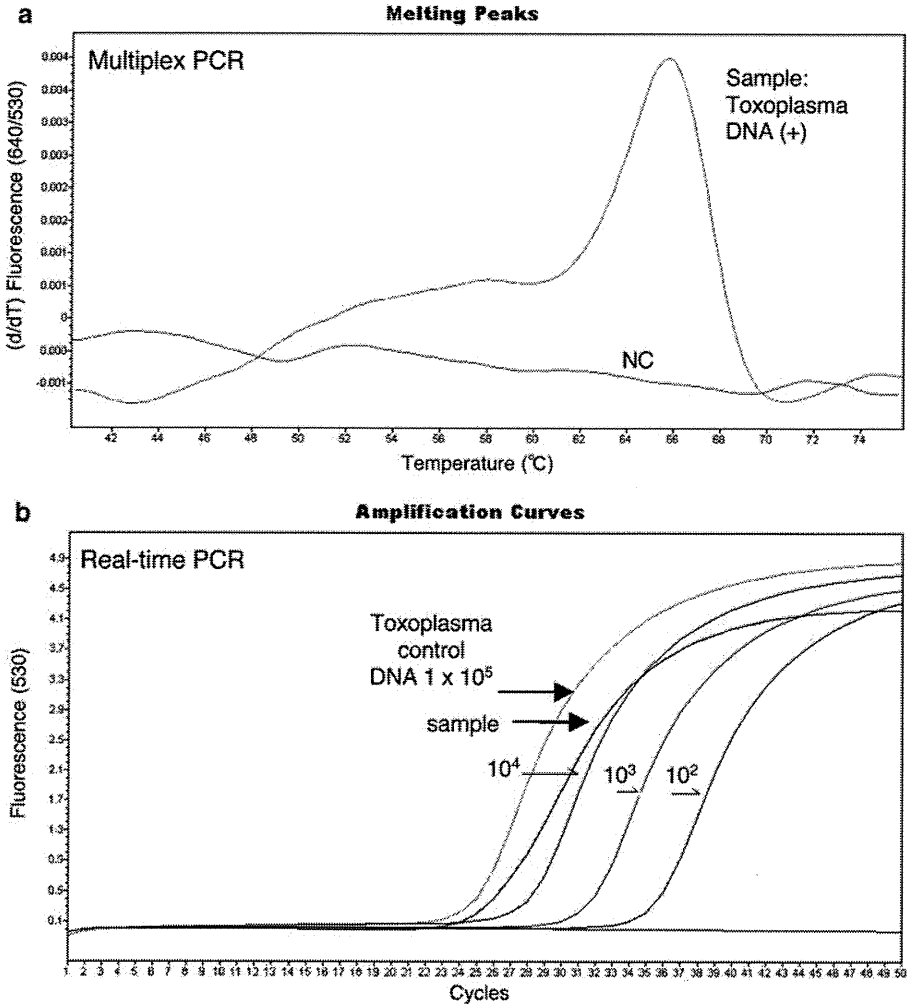

Fig. 1 PCR results for a patient with ocular toxoplasmosis (Case 1 in Table 3). **a** After DNA extraction from the sample, multiplex PCR was performed to screen for *T. gondii*, and for HHV1 to HHV8 using LightCycler capillaries. At 66°C, a significant positive curve was detected, indicating the detection of *T. gondii* genomic DNA in the aqueous humor. Using other LightCycler capillaries, human herpes viruses HSV1, HSV2, VZV, EBV, CMV, HHV6, HHV7, and HHV8 were negative for this sample. The flat line indicates the negative control. **b** Quantitative real-time PCR of the same sample shown in **a**. We calculated the copy number of the *T. gondii* genomic DNA in the sample. We measured both the tested ocular sample and control DNA (10^5, 10^4, 10^3, and 10^2 copies/mL) by real-time PCR, and then established the standard curve using the results of the control DNA. The standard curve was used to calculate the DNA concentration for the cycle threshold (*Ct*) value of the sample. The final copy number of genomic DNA in the sample (copies/mL) was calculated on the basis of the obtained sample volume and final dilution volume. Values were regarded as significant when more than 10 copies/mL were observed. The real-time PCR revealed there were 1.1×10^6 copies/mL of *T. gondii* DNA in this analyzed sample

were negative. In the serum of all of the ocular toxoplasmosis patients, the anti-toxoplasma IgG was positive (Table 3).

Negative PCR results were obtained for all the control uveitis patient samples (Cases 14–23 in Table 3) and for the control non-uveitis patients (data not shown).

Discussion

Using intraocular fluids for PCR gene amplification is helpful in diagnosing various ocular diseases, because it is possible to detect an exceedingly small amount of nucleic acid in a small ocular sample volume with high sensitivity. We report here a new PCR assay system that uses two separate steps, multiplex screening PCR and quantitative real-time PCR. With this new system, it becomes possible to detect *T. gondii* and rule out human herpes virus-related necrotizing retinitis. For these two PCR analyses in this study, oligonucleotide primers and a TaqMan probe were designed to amplify the *T. gondii* B1 gene. Our results clearly demonstrate that the PCR assay system succeeded in detecting the *T. gondii* DNA in the ocular fluid samples of the 10 patients with active ocular toxoplasmosis lesions,

Table 3 Detection of *T. gondii* DNA by qualitative multiplex PCR and quantitative real-time PCR in ocular samples from clinically suspected ocular toxoplasmosis

Case	Disease	Sample	Multiplex PCR	Real-time PCR (copies/mL)	Serum anti-Toxo IgG	Treatment
1	Toxoplasmosis (active)	AH	*T. gondii* DNA+	*T. gondii* DNA: 1.1×10^6	640	ASPM, PSL
2	Toxoplasmosis (active)	AH	*T. gondii* DNA+	*T. gondii* DNA: 1.6×10^3	320	ASPM
3	Toxoplasmosis (active)	AH	*T. gondii* DNA+	*T. gondii* DNA: 5.1×10^2	640	ASPM, PSL
4	Toxoplasmosis (active)	AH	*T. gondii* DNA+	*T. gondii* DNA: 3.0×10^4	2560	ASPM, PSL
5	Toxoplasmosis (active)	AH	*T. gondii* DNA+	*T. gondii* DNA: 9.4×10^4	5120	ASPM, PSL
6	Toxoplasmosis (active)	AH	*T. gondii* DNA+	*T. gondii* DNA: 5.5×10^4	2560	ASPM, PSL
7	Toxoplasmosis (active)	AH	*T. gondii* DNA+	*T. gondii* DNA: 9.9×10^2	640	CLDM
8	Toxoplasmosis (active)	VF	*T. gondii* DNA+	*T. gondii* DNA: 1.1×10^4	640	ASPM, PSL, PPV
9	Toxoplasmosis (active)	AH	*T. gondii* DNA+	*T. gondii* DNA: 4.2×10^3	2560	ASPM, PSL
10	Toxoplasmosis (active)	VF	*T. gondii* DNA+	*T. gondii* DNA: 2.1×10^6	1280	ASPM, PSL, PPV
11	Toxoplasmosis (old)	AH	–	<10	2560	None
12	Toxoplasmosis (old)	AH	*T. gondii* DNA+	<10	320	CLDM
13	Toxoplasmosis (old)	AH	–	<10	640	None
14	Idiopathic uveitis	AH	–	<10	320	None
15	Acute retinal necrosis	VF	VZV DNA+	VZV DNA: 8.3×10^6	<160	Valaciclovir, PPV, PSL
16	CMV retinitis	AH	CMV DNA+	CMV DNA: 9.0×10^5	<160	Ganciclovir
17	Idiopathic uveitis	AH	–	<10	<160	None
18	Idiopathic uveitis	VF	–	<10	<160	PSL, PPV
19	Idiopathic uveitis	AH	–	<10	<160	None
20	Acute retinal necrosis	AH	VZV DNA+	VZV DNA: 9.9×10^5	<160	Valaciclovir, PSL
21	Idiopathic uveitis	AH	–	<10	<160	PSL
22	Idiopathic uveitis	AH	–	<10	1280	PSL
23	Idiopathic uveitis	AH	–	<10	<160	None

We performed two PCR examinations using qualitative multiplex PCR and quantitative real-time PCR. Qualitative multiplex PCR was performed to screen for detection of the DNA of human herpes virus (HHV1-HHV8) and *T. gondii*. All samples from ocular toxoplasmosis (Cases 1–13) were negative for HHV-DNA. Anti-toxoplasma IgG was positive in the serum of all ocular toxoplasmosis patients. We collected a second ocular sample from cases 1, 2, 6, 7, 8, and 10, and performed PCR examinations. The results were all negative for DNA of human herpes virus and *T. gondii*

AH aqueous humor, *ASPM* acetylspiramycin, *CLDM* clindamycin, *PPV* pars plana vitrectomy, *PSL* prednisolone, *VF* vitreous fluids

but not in the three samples with inactive lesions. In addition, PCR did not detect any of the human herpes virus DNAs in any of the samples, nor did these PCR methods detect *T. gondii* DNA in any of the control patients. These results therefore suggest that when intraocular fluid samples are examined by a sequence of multiplex PCR and real-time PCR, the results can be used to diagnose ocular toxoplasmosis.

In this study, there was one case (Case 12 in Table 3) for which the results were positive when using qualitative multiplex PCR and negative when using quantitative real-time PCR. The qualitative PCR examination is extremely sensitive and, as such, is able to detect DNA released from inactive parasites. This may be the reason for the discrepancy seen between the qualitative and quantitative assays. However, because the amounts of intraocular DNA are so low in such patients, these situations can be regarded as innocuous. Thus, when attempting to diagnose patients, both qualitative PCR and quantitative real-time PCR should be performed to ensure that any positive results are a result of active disease and not related to older non-active lesions. When using real-time PCR, we found there was a correlation between the high DNA loads in the ocular fluids, which translates as a high copy number of *T. gondii* DNA, and the intraocular inflammation in the uveitis patients with ocular toxoplasmosis. In fact, the case that was positive when using qualitative PCR and negative when using real-time PCR (Case 12) turned out to be a patient with inactive uveitis (old pigmented retinal exudates without inflammatory signs). In this particular case, before determining the actual reason for the positivity, we did administer clindamycin to the patient in order to prevent any possible recurrence.

Although both the Goldmann–Witmer coefficient (GWC) and PCR are useful for clinical specimen analyses [1–16] and can achieve similar levels of assay sensitivity,

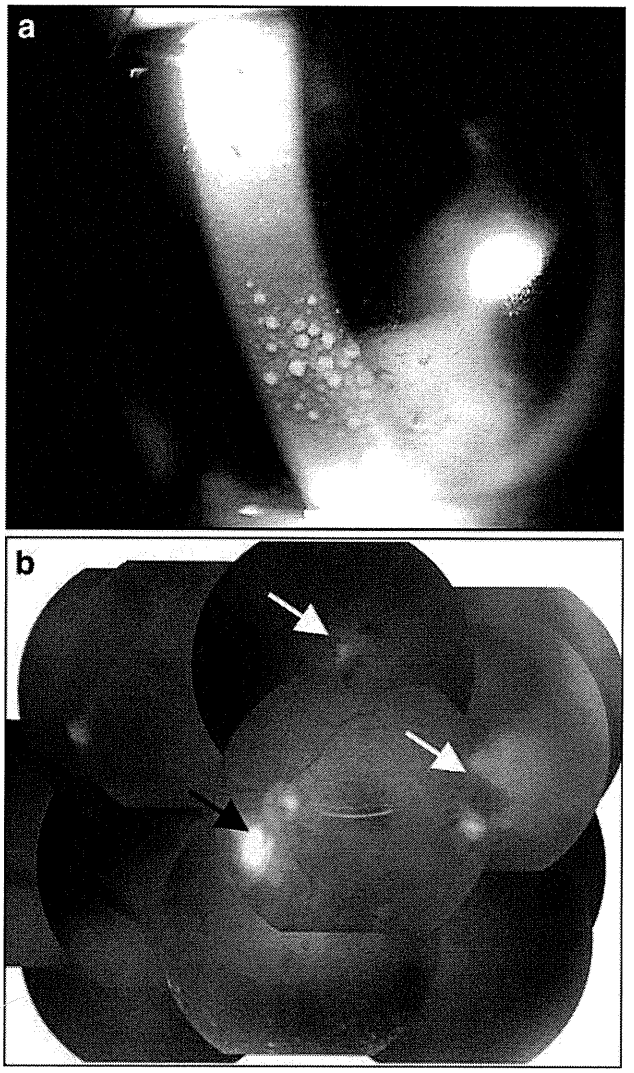

Fig. 2 Fundus and slit photograph of a patient with ocular toxoplasmosis (Case 1 in Table 3). **a** Slit and fundus photograph. **b** OS of a patient with an active toxoplasmosis infection. Diffuse keratic precipitates and anterior chamber cells (*upper panel*), and retinal yellowish white mass lesions (Edmund–Jensen type: *black arrow*) and retinal-pigmented exudates (*white arrows*) together with vitreous opacities are seen (*lower panel*)

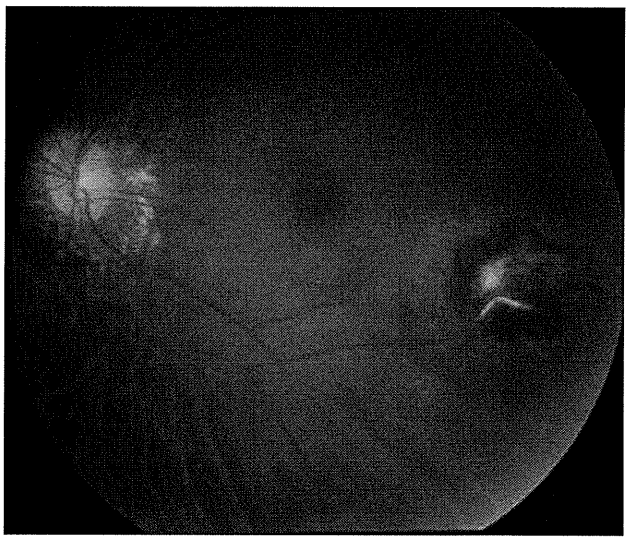

Fig. 3 A fundus photograph OS from an inactive ocular toxoplasmosis patient (Case 11 in Table 3). Old pigmented retinal exudates without inflammatory signs (vitreous cells, vitreous opacity, or retinal vasculitis) can be seen. PCR assay results were negative for genomic DNA of *T. gondii*

the proposed PCR system may be more advantageous since it has the ability to quantify the infection load of a clinical specimen. In addition, PCR examinations can exclude other major ocular infections that are caused by the human herpes virus. Westeneng et al. [7] reported 10 cases of ocular toxoplasmosis in immunocompromised patients. The PCR results were initially negative in 6 of these patients, with diagnosis only confirmed after use of the GWC. On the other hand, de Boer et al. report the use of PCR analysis was preferred for immunocompromised patients, because production of the local specific antibodies can be unpredictable in such patients [10]. Although the use of either PCR or GWC to diagnose ocular toxoplasmosis remains controversial, we were able to use PCR to detect the genomic DNA of toxoplasmosis in our immunocompetent patients even when they only had an active ocular inflammation. Therefore, this PCR methodology may be useful for *T. gondii* infection screening when used in conjunction with other diagnostic techniques, for example routine serological tests. In this study, we found increased anti-toxoplasma IgG in the serum of all of the ocular toxoplasmosis patients. However, we also found increased anti-toxoplasma IgG in the serum of two of our uveitis patients without ocular toxoplasmosis (Cases 14 and 22 in Table 3). We therefore recommend that PCR also be used to measure the toxoplasma DNA in ocular samples.

The protozoan parasite *T. gondii* has emerged as an important opportunistic infectious pathogen. In the eye, *T. gondii* infections can cause granulomatous pan-uveitis and necrotic retinitis, with typical ocular inflammation indicative of focal retinal necrosis, vitreous opacity, anterior chamber cells, and choroidal edema. Fundus lesions seen in ocular toxoplasmosis can be atypical in many patients, resembling necrotizing retinitis caused by human herpes viruses. The new PCR method is particularly useful when screening those uveitis patients who usually fail to generate specific IgM or increased IgG titers for *T. gondii* or who have had focal retinal necrosis. Thus, these results can be used to distinguish the findings from other retinal necrotic disorders, for example acute retinal necrosis and cytomegalovirus retinitis. By using several different primer pairs in LightCycler capillaries, these methods proved capable of rapidly screening for detection of the genome of

all eight types of human herpes virus and *T. gondii*. Development of this multiplex and real-time PCR assay seems to be quite advantageous, because this methodology makes it possible to exclude non-toxoplasma uveitis patients.

In conclusion, we have established a rapid, sensitive, comprehensive, two-step PCR system that can be used to detect *T. gondii*. New studies that examine larger numbers of samples from suspected ocular toxoplasmosis patients will need to be undertaken in the future in order to definitively establish the clinical value of this new diagnostic technique.

Acknowledgments Drs Kazuichi Maruyama and Kenji Nagata of the Department of Ophthalmology, Kyoto Prefectural University of Medicine, collected and sent the samples used in this study. We are grateful for the expert technical assistance of Mr Ken Watanabe. This work was supported by Comprehensive Research on Disability, Health and Welfare, Health and Labour Sciences Research Grants, Ministry Health, Labour and Welfare, Japan.

References

1. Aouizerate F, Cazenave J, Poirier L, Verin P, Cheyrou A, Begueret J, et al. Detection of *Toxoplasma gondii* in aqueous humour by the polymerase chain reaction. Br J Ophthalmol. 1993;77:107–9.
2. Manners RM, O'Connell S, Guy EC, Joynson DH, Canning CR, Etchells DE. Use of the polymerase chain reaction in the diagnosis of acquired ocular toxoplasmosis in an immunocompetent adult. Br J Ophthalmol. 1994;78:583–4.
3. Robert-Gangneux F, Binisti P, Antonetti D, Brezin A, Yera H, Dupouy-Camet J. Usefulness of immunoblotting and Goldmann–Witmer coefficient for biological diagnosis of toxoplasmic retinochoroiditis. Eur J Clin Microbiol Infect Dis. 2004;23:34–8.
4. De Groot-Mijnes JD, Rothova A, Van Loon AM, Martinus RA, Völker R, ten Dam-van Loon NH, et al. Polymerase chain reaction and Goldmann–Witmer coefficient analysis are complimentary for the diagnosis of infectious uveitis. Am J Ophthalmol. 2006;141:313–8.
5. Kijlstra A, Luyendijk L, Baarsma GS, Rothova A, Schweitzer CM, Timmerman Z, et al. Aqueous humor analysis as a diagnostic tool in toxoplasma uveitis. Int Ophthalmol. 1989;13:383–6.
6. Witmer R. Clinical implications of aqueous humor studies in uveitis. Am J Ophthalmol. 1978;86:39–44.
7. Westeneng AC, Rothova A, de Boer JH, de Groot-Mijnes JD. Infectious uveitis in immunocompromised patients and the diagnostic value of polymerase chain reaction and Goldmann–Witmer coefficient in aqueous analysis. Am J Ophthalmol. 2007;144:781–5.
8. Matos K, Muccioli C, Belfort Junior R, Rizzo LV. Correlation between clinical diagnosis and PCR analysis of serum, aqueous, and vitreous samples in patients with inflammatory eye disease. Arq Bras Oftalmol. 2007;70:109–14.
9. Rothova A, de Boer JH, Ten Dam-van Loon NH, Postma G, de Visser L, Zuurveen SJ, et al. Usefulness of aqueous humor analysis for the diagnosis of posterior uveitis. Ophthalmology. 2008;115:306–11.
10. de Boer JH, Verhagen C, Bruinenberg M, Rothova A, de Jong PT, Baarsma GS, et al. Serologic and polymerase chain reaction analysis of intraocular fluids in the diagnosis of infectious uveitis. Am J Ophthalmol. 1996;121:650–8.
11. Figueroa MS, Bou G, Marti-Belda P, Lopez-Velez R, Guerrero A. Diagnostic value of polymerase chain reaction in blood and aqueous humor in immunocompetent patients with ocular toxoplasmosis. Retina. 2000;20:614–9.
12. Bottós J, Miller RH, Belfort RN, Macedo AC, UNIFESP Toxoplasmosis Group, Belfort R Jr, et al. Bilateral retinochoroiditis caused by an atypical strain of *Toxoplasma gondii*. Br J Ophthalmol. 2009;93:1546–50.
13. Lin MH, Chen TC, Kuo TT, Tseng CC, Tseng CP. Real-time PCR for quantitative detection of *Toxoplasma gondii*. J Clin Microbiol. 2000;38:4121–5.
14. Patrat-Delon S, Gangneux JP, Lavoué S, Lelong B, Guiguen C, le Tulzo Y, et al. Correlation of parasite load determined by quantitative PCR to clinical outcome in a heart transplant patient with disseminated toxoplasmosis. J Clin Microbiol. 2010;48:2541–5.
15. Fekkar A, Bodaghi B, Touafek F, Le Hoang P, Mazier D, Paris L. Comparison of immunoblotting, calculation of the Goldmann–Witmer coefficient, and real-time PCR using aqueous humor samples for diagnosis of ocular toxoplasmosis. J Clin Microbiol. 2008;46:1965–7.
16. Cassaing S, Bessières MH, Berry A, Berrebi A, Fabre R, Magnaval JF. Comparison between two amplification sets for molecular diagnosis of toxoplasmosis by real-time PCR. J Clin Microbiol. 2006;44:720–4.
17. Sugita S, Shimizu N, Watanabe K, Mizukami M, Morio T, Sugamoto Y, et al. Use of multiplex PCR and real-time PCR to detect human herpes virus genome in ocular fluids of patients with uveitis. Br J Ophthalmol. 2008;92:928–32.
18. Sugita S, Iwanaga Y, Kawaguchi T, Futagami Y, Horie S, Usui T, et al. Detection of herpesvirus genome by multiplex polymerase chain reaction (PCR) and real-time PCR in ocular fluids of patients with acute retinal necrosis. Nippon Ganka Gakkai Zasshi. 2008;112:30–8.
19. Sugita S, Shimizu N, Watanabe K, Katayama M, Horie S, Ogawa M, et al. Diagnosis of bacterial endophthalmitis by broad-range quantitative polymerase chain reaction. Br J Ophthalmol. 2011;95:345–9.

Graefes Arch Clin Exp Ophthalmol (2012) 250:391–398
DOI 10.1007/s00417-011-1819-1

INFLAMMATORY DISORDERS

Detection of *Candida* and *Aspergillus* species DNA using broad-range real-time PCR for fungal endophthalmitis

Sunao Sugita · Koju Kamoi · Manabu Ogawa · Ken Watanabe · Norio Shimizu · Manabu Mochizuki

Received: 24 June 2011 / Revised: 29 August 2011 / Accepted: 2 September 2011 / Published online: 27 September 2011

Abstract
Background The goal of this work is to establish a broad-range real-time polymerase chain reaction (PCR) diagnostic system for ocular fungal infection and to measure *Candida* and *Aspergillus* DNA in the ocular fluids obtained from unknown uveitis/endophthalmitis patients.
Methods After obtaining informed consent, intraocular fluids (aqueous humor and vitreous fluid samples) were collected from 54 patients with idiopathic uveitis or endophthalmitis. Samples were assayed for *Candida* or *Aspergillus* DNA using broad-range (18S rRNA sequences) quantitative real-time PCR.
Results *Candida* or *Aspergillus* DNA was detected in seven out of 54 patient ocular samples (13%). These PCR-positive samples showed significantly high copy numbers of *Candida* or *Aspergillus* DNA. On the other hand, fungal DNA was not detected in any of the other 46 samples collected from these idiopathic uveitis or endophthalmitis patients. In the one PCR-negative case, PCR did not detect any fungal genome in the sample, even though this patient was clinically suspected of having *Candida* endophthalmitis. Real-time PCR results were negative for fungal DNA in the bacterial endophthalmitis patients and in various uveitis patients. In addition, fungal DNA was also not detected in patients without ocular inflammation (controls).
Conclusions Analysis of ocular samples by this broad-range real-time PCR method can be utilized for rapid diagnosis of patients suffering from unknown intraocular disorders such as idiopathic uveitis/endophthalmitis.

Keywords Endophthalmitis · Fungal infection · Polymerase chain reaction

S. Sugita (✉) · K. Kamoi · M. Ogawa · M. Mochizuki
Department of Ophthalmology & Visual Science,
Tokyo Medical and Dental University,
Graduate School of Medical and Dental Sciences,
1-5-45 Yushima,
Bunkyo-ku, Tokyo 113-8519, Japan
e-mail: sunaoph@tmd.ac.jp

K. Watanabe · N. Shimizu
Department of Virology, Division of Medical Science,
Tokyo Medical and Dental University,
Graduate School of Medical and Dental Sciences,
Tokyo, Japan

Introduction

Fungal endophthalmitis is a sight-threatening disease caused by human pathogenic fungi. Fungal infections are known to cause ocular inflammations such as endophthalmitis, uveitis, and keratitis. However, with the exception of for the *Candida*-associated ocular infection, the association between the fungus and the observed clinical features has yet to be elucidated. The well-known clinical features for *Candida* endophthalmitis include a fungal ball in the retina and vitreous opacity [1]. Fungal endophthalmitis can result from hematogenous dissemination or from a direct inoculation following trauma or surgery to the eye. Risk factors for fungal endophthalmitis include intravascular catheters, diabetes, malignancy, chemotherapeutic agents, and steroids. However, the clinical findings can be very diverse in some cases of ocular inflammatory disorders caused by fungal species. Moreover, fungal infections have been widely associated with keratitis, retinitis, uveitis, retinal/choroidal vasculitis, invasive orbital infection, and endophthalmitis. Because of this diversity, infection diagnosis is both difficult and time-consuming [1–4]. In order to be able to perform adequate treatments that can prevent these infectious agents from causing irreversible ocular damage,

early examinations that correctly identify the etiology of the infection are necessary.

Conventional methods of diagnosis of fungal endophthalmitis include detection and isolation of the fungi from the intraocular fluids (aqueous humor or vitreous). However, since the sensitivity of conventional fungal cultures is not high, and the culture growth rates are slow, longer times are required before final results can be obtained [5, 6]. Thus, an early diagnosis can be important in ensuring there is prompt management of the endophthalmitis. Previous studies have shown that polymerase chain reaction (PCR) can be successfully and reliably used to make a diagnosis of fungal endophthalmitis [7–10]. However, even conventional PCR has yet to be able to determine quantitative information for the fungal genome in ocular samples.

In this study, we used real-time quantitative PCR for detection of *Candida* and *Aspergillus* DNA. We developed a protocol for the rapid detection of fungal DNA in ocular samples that was based on two major species (*Candida* and *Aspergillus*) that commonly cause eye disorders. We designed novel panfungal primers and probes that were complementary to the 18S rRNA sequences present in these species. Our broad-range real-time PCR proved to be an accurate method for quantitating fungal copies of both *Candida* and *Aspergillus* DNA.

Methods

Sample preparation

From 2006 to 2010, we consecutively enrolled endophthalmitis and uveitis patients in a prospective study that was conducted at our hospital (Table 1). After informed consent was obtained in all patients, we collected aqueous humor and vitreous fluid samples. A 0.1–0.2 ml aliquot of aqueous humor (asepsis) was collected in a syringe with a 30-G needle. We also collected non-diluted vitreous fluid samples (0.5–1.0 ml) during diagnostic pars plana vitrectomy (PPV) procedures that were conducted in patients with clinically suspected fungal endophthalmitis/uveitis. All of the patients displayed active intraocular inflammation at the time of sampling. The samples were transferred into a pre-sterilized microfuge tube and used for PCR. To ensure that no contamination of the PCR preparation occurred, the DNA amplification and the analysis of the amplified products were done in separate laboratories, as per a method reported for one of our previous studies [11].

For cultures of fungi, the Bacteria Work Station of the Tokyo Medical and Dental University Hospital processed all specimens (aqueous humor and vitreous fluids) within 1 h after the sample collection, with standard methods followed for the isolation and identification of fungal cultures [11].

In addition to the patient groups, we also analyzed samples from a control group. A total of 40 samples (20 aqueous humor and 20 vitreous fluids) were collected from patients who did not have any type of ocular inflammation (age-related cataract, macular edema, retinal detachment, idiopathic macular hole, or idiopathic epiretinal membrane).

The research followed the tenets of the Declaration of Helsinki and all study protocols were approved by the Institutional Ethics Committee of Tokyo Medical and Dental University. This clinical trial was registered, with registration information available at www.umin.ac.jp/ctr/index/htm. The study number attached to this registration is R000002708. The study was begun in April of 2006 and ended in April of 2010.

Polymerase chain reaction

To detect the *Candida* and *Aspergillus* DNA, we designed primers and probes for the broad-range PCR of the 18S rRNA sequences, which we have described in a previous report [10]. Kami et al. [12] developed primers and a probe for real-time PCR and demonstrated that the procedure was highly specific for the *Aspergillus* infection. In this study, we also designed a probe for use in the *Candida* species DNA amplifications (Fig. 1).

DNA was extracted from the samples using a DNA Mini Kit (Qiagen, Valencia, CA) installed on a robotic workstation that was set for automated purification of nucleic acids (BioRobot E21, Qiagen). The real-time PCR was performed using the Amplitaq Gold and the Real-Time PCR 7300 system (Applied Biosystems, Foster City, CA) or Light Cycler 480 II (Roche, Switzerland). The paired primers and TaqMan probes used for *Candida* and *Aspergillus* are shown in Fig. 1. Products were subjected to 50 cycles of PCR amplification, with cycling conditions set at 95°C for 10 min, followed by 50 cycles at 95°C for 15 s and 60°C for 1 min. For PCR assay sensitivity, PCR fragments were amplified from the DNA of *C. albicans* (Strain: ATCC 60193). Amplification of the human β-globulin gene served as an internal positive extraction and amplification control. Copy number values of more than ten copies/ml in the sample were considered to be significant.

Results

Specificity of *Candida* and *Aspergillus* species in broad-range real-time PCR

To evaluate the specificity of the *Candida* and *Aspergillus* species using broad-range real-time PCR of the 18S rRNA sequences, total nucleic acids of six *Candida* species and five *Aspergillus* species were extracted and assayed for 18S

Table 1 Detection of *Candida* and *Aspergillus* 18S rRNA gene by broad-range real-time PCR in unknown uveitis or endophthalmitis patients and control uveitis patients

Initial diagnosis	No. of patients	Sample	Results for real-time PCR	Final diagnosis	Remarks
Idiopathic uveitis/ endophthalmitis	n=46	Aqh, VF	<10 copies	Idiopathic uveitis/ endophthalmitis	
	n=1 (65, male)	VF	*Candida* 9.2×10^5 copies/ml	*Candida* endophthalmitis	Case 1; Endogenous endophthalmitis
	n=1 (71, female)	VF	*Aspergillus* 4.5×10^2 copies/ml	*Aspergillus* endophthalmitis	Case 2; Endogenous endophthalmitis
	n=1 (73, male)	VF	*Aspergillus* 1.8×10^3 copies/ml	*Aspergillus* endophthalmitis	Case 3; Late postoperative endophthalmitis
	n=1 (80, male)	Aqh	*Candida* 3.4×10^2 copies/ml	*Candida* endophthalmitis	Case 4; Post-traumatic corneal ulceration
	n=1 (66, female)	VF	*Candida* 6.5×10^5 copies/ml	*Candida* endophthalmitis	Case 5; Endogenous endophthalmitis (IFN treatment)
	n=1 (74, male)	VF	*Candida* 6.2×10^4 copies/ml	*Candida* endophthalmitis	Case 6; Endogenous endophthalmitis (diabetes)
	n=1 (0, female)	VF	*Candida* 9.4×10^4 copies/ml	*Candida* endophthalmitis	Case 7; Endogenous endophthalmitis (normal infant)
	n=1 (60, male)	Aqh	<10 copies	*Candida* endophthalmitis	Case 8; Endogenous endophthalmitis (IVH use)
Bacterial endophthalmitis	n=7	Aqh, VF	<10 copies	/	
Sarcoidosis	n=4	Aqh, VF	<10 copies	/	
Vogt-Koyanagi-Harada disease	n=1	Aqh	<10 copies	/	
Toxocariasis	n=1	Aqh	<10 copies	/	
Toxoplasmosis	n=3	Aqh, VF	<10 copies	/	
Acute retinal necrosis	n=7	Aqh, VF	<10 copies	/	
Cytomegalovirus retinitis	n=4	Aqh, VF	<10 copies	/	
Herpetic anterior iridocyclitis	n=4	Aqh	<10 copies	/	
Non-inflammatory ocular diseases*	n=40	Aqh, VF	<10 copies	/	Controls for PCR

*Non-inflammatory ocular diseases: age-related cataract, macular edema, retinal detachment, idiopathic macular hole or idiopathic epiretinal membrane

Aqh aqueous humor, *IFN* interferon, *IVH* Intravenous hyperalimentation, *VF* vitreous fluids

rDNA. As seen in Fig. 1, the broad-range real-time PCR detected six *Candida* species, i.e., *C. albicans, C. parapsilosis, C. tropicalis, C. guilliermondii, C. glabrata,* and *C. krusei*, along with five *Aspergillus* species, i.e., *A. fumigatus, A. flavus, A. nidulans, A. niger,* and *A. terreus*. By using several different primers and probes, we were able to separately detect each of these fungal species (Fig. 1).

Sensitivity of the real-time PCR assay

To confirm the broad-range real-time PCR assay sensitivity, PCR fragments were amplified from the DNA of *C. albicans*. The detection limit and standard range of the TaqMan real-time PCR were determined by using serial tenfold dilutions of linearized plasmid. The PCR results for the prepared samples showed that the best sensitivity for detecting *C. albicans* DNA was at a concentration of 10^1 per PCR (Fig. 2). There was no detection of the DNA in the negative control (nuclease-free water).

Detection of *Candida* and *Aspergillus* 18S rRNA gene in unknown uveitis/endophthalmitis patients

PCR results indicated a total of seven ocular fluid samples from the idiopathic uveitis or endophthalmitis patients (7/54, 13% positive, Table 1) were positive for *Candida* or *Aspergillus* DNA. These positive patients had high copy numbers of either *Candida* or *Aspergillus* DNA, with values ranging from 3.4×10^2 to 9.2×10^5 copies/ml. These results indicate the presence of a fungal infection. A representative PCR result is shown in Fig. 3. Conversely, conventional fungal cultures only found two out of the seven PCR-positive samples (both *C. albicans*) to be positive, while the other five samples were negative.

On the other hand, fungal DNA was not detected in any of the other 46 samples collected from these idiopathic uveitis or endophthalmitis patients. In the one PCR-negative case, PCR did not detect any fungal genome in the aqueous humor (<10 copies, case 8 in Table 1), even

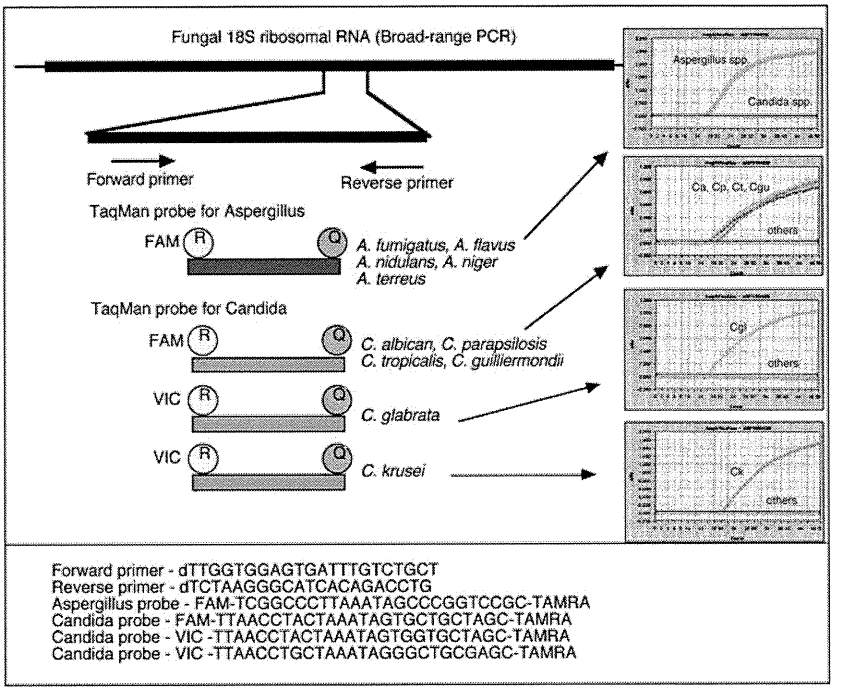

Fig. 1 Specific primers and probes for broad-range real-time PCR of the fungal 18S rRNA sequence were designed in order to detect DNA for *Candida* and *Aspergillus* species

though this patient was clinically suspected of having *Candida* endophthalmitis. Real-time PCR results were negative for the *Candida* and *Aspergillus* DNA in the bacterial endophthalmitis patients (n=7) and in the various uveitis patients (n=24) who had been diagnosed with sarcoidosis, Vogt-Koyanagi-Harada disease, toxocariasis, toxoplasmosis, acute retinal necrosis, cytomegalovirus retinitis, or herpetic anterior iridocyclitis. In addition, fungal DNA was not detected in any of the 40 control samples that were collected from the patients without ocular inflammation.

Of the seven patients who were PCR positive, further examinations led to fungal endophthalmitis diagnoses as follows: five patients had endogenous endophthalmitis (four *Candida* and one *Aspergillus*), one had late postoperative endophthalmitis (*Aspergillus*, case 3), and one had post-traumatic keratitis-associated endophthalmitis (*Candida*, case 4) (Table 1).

Case reports

Case 1

A 65-year-old man with type II diabetes mellitus was treated for unknown uveitis over a period of a few weeks during 2009. He complained of blurred vision, decreased visual acuity, and pain in his right eye (RE). Ophthalmologic examination demonstrated the presence of characteristics of uveitis, bacterial endophthalmitis and fungal endophthalmitis. Vitreous opacity, including the presence of a fungal ball and yellowish retinal exudates, was seen in the fundus of his RE (Fig. 4a). After vitrectomy of his RE,

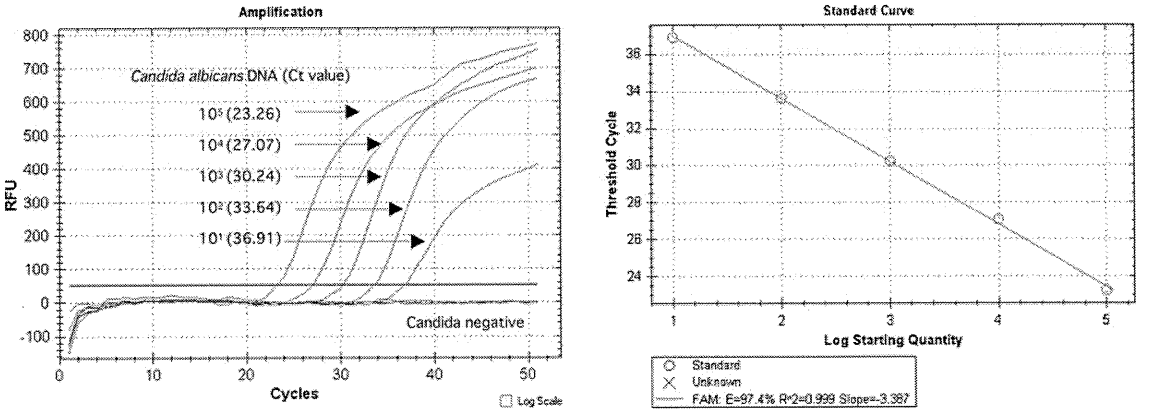

Fig. 2 In order to examine broad-range real-time PCR assay sensitivity for the fungal 18S PCR, the PCR fragments were amplified from the DNA of *C. albicans* (ATCC 60193). The *number in parenthesis* indicates the cycle threshold (Ct) value in quantitative PCR

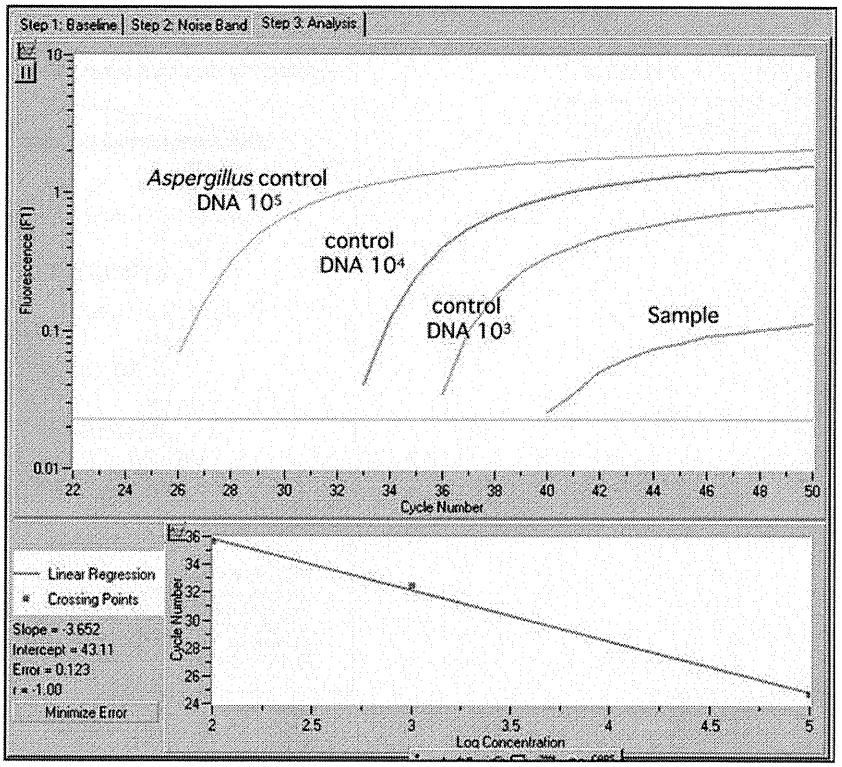

Fig. 3 Representative data for the broad-range real-time PCR. *Aspergillus* DNA (4.5×10^2 copies/ml) but not *Candida* DNA was detected in the vitreous sample of case 2

real-time PCR of the vitreous sample obtained during the procedure indicated there were high copy numbers of *Candida* DNA (9.2×10^5 copies/ml, Fig. 4b). Based on these results, the patient was given systemic fluconazole (Table 1). *Aspergillus* DNA was not detected in this sample. A few days later, fungal culture of his vitreous specimen

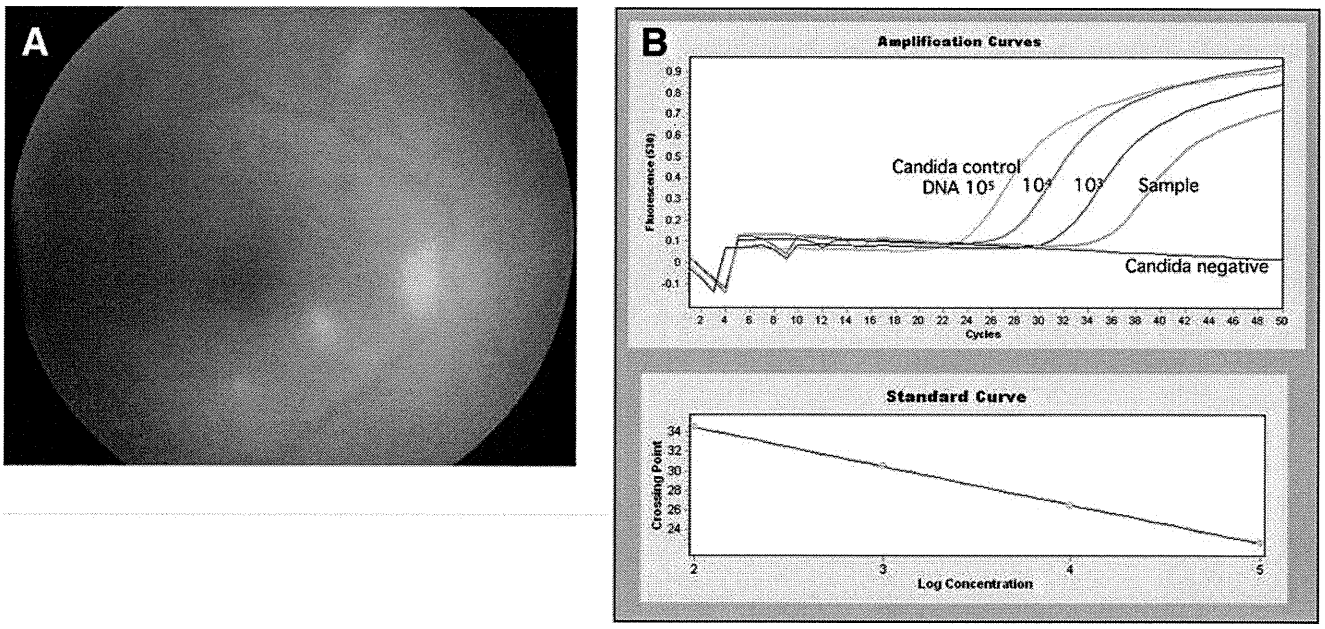

Fig. 4 PCR results for case 1. **a** Fundus photograph of the right eye with a *Candida* infection. Dense vitreous opacity and retinal exudates are seen. **b** This is a graph of the PCR results. We calculated the copy number of fungal genomic DNA in the sample. After we measured both the tested ocular sample and the control DNA (10^5, 10^4, and 10^3 copies/ml) using real-time PCR, we then established the standard curve based on the results of the control DNA. Based on this standard curve, the sample Ct value was used to determine the DNA concentration of the sample. Final copy numbers of genomic DNA in the sample (copies/ml) were calculated based on the obtained sample volume and final dilution volume. High copy numbers of *Candida* DNA (9.2×10^5 copies/ml) were detected by PCR. *Aspergillus* DNA was not detected in the sample